NASA-CR-191274

Department of Aerospace Engineering
The Pennsylvania State University
University Park, PA 16802

ANALYSIS AND DESIGN OF PLANAR AND NON-PLANAR WINGS FOR INDUCED DRAG MINIMIZATION

FINAL PROGRESS REPORT

NASA Grant NAG-1-1198

ATTN; Raymond E. Mineck
Technical Monitor

Karl W. Mortara, Dennis M. Straussfogel, and Mark D. Maughmer

Department of Aerospace Engineering
The Pennsylvania State University
University Park, PA 16802

November 1992

Table of Contents

I. Summary

The goal of the work reported herein is to develop and validate computational tools to be used for the design of planar and non-planar wing geometries for minimum induced drag. Because of the iterative nature of the design problem, it is important that, in addition to being sufficiently accurate for the problem at hand, these tools need to be reasonably fast and computationally efficient. Toward this end, a method of predicting induced drag in the presence of a free wake has been coupled with a panel method. The induced drag prediction technique is based on the application of the Kutta-Joukowski law at the trailing edge. Until now, the use of this method has not been fully explored and pressure integration and Trefftz-plane calculations favored. As is shown in this report, however, the Kutta-Joukowski method is able to give better results for a given amount of effort than the more commonly used techniques, particularly when relaxed wakes and non-planar wing geometries are considered. Using these methods, it is demonstrated that a reduction in induced drag can be achieved through non-planar wing geometries. It remains to determine what overall drag reductions are possible when the induced drag reduction is traded-off against increased wetted area. With the design methodology that is described herein, such trade studies can be performed in which the non-linear effects of the free wake are taken into account.

II. Introduction

As the practical application of laminar flow control to commercial transport aircraft comes closer and closer to realization, in order to gain the full benefit of this technology, it is important in the wing design process that it be balanced with induced and wave drag considerations such that the overall wing drag is minimized. Toward this end, the research effort reported herein has been directed to the prediction and minimization of induced drag. Recently reported findings have indicated that induced drag may be reduced by utilizing unconventionally shaped and/or non-planar wing planforms[1-3]. To validate these findings, it is necessary to be able to predict the induced drag with reliability and precision. Furthermore, if the same method is to be used for design purposes then, because of the iterative nature of the design process, it is also necessary that the method be computationally efficient. Thus, an analysis method has been developed which has the accuracy of a higher-order panel method using a large panel density, while requiring only a small percentage of the computational time. The technique is capable of accounting for the effects of a free wake in the prediction of the induced drag for both planar and non-planar wings.

Because the difficulties which accompany theoretical induced drag predictions are also present experimentally, validation of induced drag prediction methods is extremely difficult. Unfortunately, because of this, such validation must largely be based on comparison with predictions of other theoretical methods. For this purpose, the methods used for such comparisons are in widespread use and well calibrated.

At this point, the newly developed method for predicting induced drag has been validated by comparing its predictions with those of other commonly used analysis schemes. It has also been used to match the experimental results of a recent wind-tunnel test directed at exploring the influence of planform geometry on induced drag. In both exercises, the new method performed very well.

III. Background Discussion

To calculate the induced drag generated by a lifting surface it is required that all, or at least part, of the velocity field be determined in the vicinity of the wing. Potential flow methods generally solve for the velocity over only a small part of the flow field and thereby save a tremendous amount of computation time. The induced drag is calculated in these methods by either applying the Kutta-Joukowski law to the bound vorticity, or by integrating the streamwise components of pressure on the surface of the wing. For this reason, potential flow methods require solution of the velocity field only at points on the lifting surface as opposed to points over the entire flow field. The potential flow methods which employ the Kutta-Joukowski law determine the downwash velocity at the wing either by direct calculation, or by analyzing the flow in the far-wake where the flow is assumed to be two-dimensional (i.e., in the Trefftz plane) and relating that solution to the flow at the wing. The latter technique assumes the wake of the wing to be rigid and aligned with the free-stream velocity.

A more computationally intensive approach for calculating the induced drag is to solve the Euler or Navier-Stokes equations over the entire flow field. The induced drag is then determined by integrating the resulting distributed pressure force on the wing surface, or directly from the calculated vorticity shed into the wake. The amount of computer time required to solve the governing equations makes this approach impractical as a tool for preliminary design, although it has the potential for being extremely valuable for the accurate analysis of a given geometry.

The following is a brief explanation of available methods for calculating induced drag and a discussion of the strengths and weaknesses of a number of potential flow methods, as well as methods which make use of the Euler or Navier-Stokes equations.

Lifting-Line Theory (Prandtl-Lanchester)

The lifting-line theory of Prandtl analyzes the flow field as a potential field with the wing modeled as a line vortex of varying strength located at the wing quarter-chord[4]. Helmholtz's theorem requires that any spanwise change in vorticity of the lifting line be shed into a sheet of distributed trailing vorticity. The trailing vorticity is assumed to be aligned with the free-stream velocity and to extend downstream to infinity. The strength of the trailing vortex sheet at any spanwise location is equal to the spanwise change in vortex strength at the corresponding point on the lifting line. In this model, the sheet of trailing vorticity is assumed to be rigid and does not deform under its own induced velocity. The velocity that the trailing vortex sheet induces on the lifting line is used to calculate the induced drag of the wing.

Munk made use of the lifting-line theory to calculate the optimum spanwise lift distribution for minimum induced drag within the context of the given assumptions[5]. In this case, the minimum induced drag is achieved when the induced velocity normal to the lifting line is proportional to the cosine of the local dihedral angle. For a straight lifting line (dihedral angle equal to zero everywhere along the span) the classical result of a constant downwash over the span, as generated by an elliptical lift distribution, is obtained. For a curved lifting line, which models a non-planar wing with spanwise varying dihedral angle, the optimum lift distribution for minimum induced drag is well defined, again, within the limits of the given assumptions[6]. Several questions arise, however, regarding the assumptions used in obtaining these results. In particular, the lifting-line model ignores the effect of the chordwise distribution of vorticity on the downwash distribution since all the vorticity generated at a given spanwise location has been collapsed to a single point. Also, the effect that the deforming wake has on wing performance is not taken into account. While lifting-line theory is useful for approximating the performance of unswept, high-aspect-ratio wings once the chord distribution is fixed, the method is unable to account for any aerodynamic differences between wings due to different planform shapes.

Modified Lifting-Line Theory (Eppler)

A recent modification to lifting-line theory locates the non-planar lifting line along the trailing edge of the planform instead of along the quarter-chord line[7]. As in the Prandtl lifting-line model, the effects of chordwise loading are not included; however, the influence of the trailing-edge shape is now considered. It is assumed in this method that the bound vorticity does not influence the induced velocity at the lifting line and is therefore not considered in any downwash calculations. Induced drag is calculated in this method by applying the Kutta-Joukowski law to the bound vorticity at the trailing edge. The method can be implemented with either fixed- or free-wake analyses, and can consider planar and non-planar wing planforms. In the standard lifting-line model, the lifting line is placed at the quarter-chord to be in agreement with the two-dimensional lumped-vortex element approach in which this positioning properly matches pitching moment results and effectively satisfies the Kutta condition. For the computation of induced drag, however, calculating the downwash at this point is not consistent with the physics of the problem. As the wing must pass before any actual downwash can occur, the tailing edge placement of the lifting line used in the modified theory provides a better model for induced drag calculations than that of the classical approach. In this way, although much of the simplicity of the Prandtl model is retained, the modified lifting-line method can account for some planform effects through the shape of the trailing edge.

Vortex-Lattice Methods

Vortex-lattice methods[8] make use of an array of horseshoe vortices with spanwise segments bound to the wing and streamwise segments trailing downstream from the trailing edge parallel to the free-stream velocity. The strength of each vortex is determined by satisfying the condition that the flow be tangent to the mean camber line of the wing at a number of control points equal to the number of vortices used. This constraint defines a system of simultaneous linear equations which are solved for the vortex strengths. The strengths of the streamwise trailing vortex filaments are taken as the sum of the strengths of the horseshoe vortices distributed over the chord at a given spanwise position.

Modeling the wing using the vortex-lattice approach attempts to capture the effect of the chord-wise loading on the overall wing aerodynamics, although thickness effects are ignored. Typically the wing wake is modeled using straight, non-deforming vortex filaments aligned with the free stream; however, the effect of the deforming wake can be included in this method using wake relaxation[9].

Induced drag is normally calculated in the vortex-lattice method by applying the Kutta-Joukowski law on the spanwise bound vortex segments which are in the influence of the local downwash. Consequently, the orientation of the bound vortices is important and some research has been done regarding the way in which the lattice is constructed[10-13]. One question which arises is whether or not the spanwise vortex segments should be aligned perpendicular to the free-stream velocity, aligned with the sweep angle of the wing, or aligned in some other direction depending on the wing planform shape. Unfortunately, it is found that the choice of lattice shape can have a significant effect on the solutions and the answer to the above question actually depends on what information is being sought.

Linear Panel Methods

Panel methods discretize the wing upper and lower surfaces into source, doublet, or vortex panels which induce a perturbation on the uniform (free-stream) velocity field[14]. Unlike vortex-lattice methods, such methods consider the effects of wing thickness. Low-order panel methods assume the panels to be flat with constant singularity strength over the entire panel[15], while higher-order methods consider surface curvature and allow for a distribution of source, doublet, or vortex strength over the panel. The strength of the singularity on each panel is determined by satisfying the flow tangency condition at a number of control points that is equal to the number of panels used. As in the vortex-lattice method, the application of the appropriate boundary conditions produces a system of linear simultaneous equations that are solved for the panel strengths. The shape of the freely deforming wake can also be computed by discretizing the wake into panels and calculating the flow velocity at each panel. The wake is then reoriented so that each panel is aligned with the local velocity vector. Since the singularity strength and orientation of the panels in the wake effect those on the wing, this process must be iterated until it converges and a steady-state wake shape is obtained.

For panel methods, induced drag can be calculated by taking the streamwise component of the product of surface pressure and panel area summed over all the wing panels. This method is extremely sensitive to errors in the calculated pressure distribution which are most pronounced near the leading edges and wing tips, even in higher-order methods[3]. Another means of calculating induced drag is to either assume a rigid wake, or attempt to compute the deformed wake shape, and numerically integrate the so-called "Trefftz-plane" integral over the velocity field far downstream where the flow is assumed to be two-dimensional. In the relaxed-wake case, this approach is not practical because in order to resolve the velocities well enough, the singular vortex filaments are approached so closely that the validity of the induced drag calculation becomes questionable.

Full-Potential, Euler and Navier-Stokes Methods

Linearized potential flow methods do not include the effects of compressibility and are therefore inadequate for the transonic wing design problem. To take these effects into account, solution of the full potential, Euler, or Navier-Stokes equations is required. The solution must be computed over a large enough region of the flow so that the significant upstream and downstream effects on the wing performance are captured. As in the linearized case, the full-potential equation requires that the wake geometry be specified, or fitted, as a boundary condition before solution takes place[16]. In the case of the Euler or Navier-Stokes equations, the freely deforming wake shape is captured in the solution. Once the velocity distribution on the wing is determined, the lift and induced drag can be found from a surface pressure integration similar to that used in panel methods. Determining lift and drag from a far-field wake-integration scheme has also been attempted with some success[17].

In order to numerically solve the Euler equations for a simple wing geometry over the number of grid points needed for reasonable accuracy, several hours of computation time on a CRAY Y-MP are required[17]. Solution of the full-potential equation would require a similar effort[18]. While not unreasonable for analysis purposes, this amount of computational time is generally considered excessive for use in an iterative design process.

To include both the effects of viscosity and compressibility in the wing design problem, either a boundary-layer solution would have to be interacted with the full potential or Euler solution, or the full Navier-Stokes equations would have to be used. As this would require an amount of computation time even greater than that required for the Euler equations, this approach is also considered to be impractical for routine design activities.

A Note on Calculating the Deformed Wake Shape

Due to the mathematical instability inherent in the self-induced motion of a vortex sheet, an accurate determination of the shape of a freely deforming wake in any potential flow technique is an extremely difficult problem. Spacial relaxation methods calculate the local velocity at points in the wake, align the trailing vortex filaments with the local velocity (streamlines), and then iterates until convergence to a steady state wake shape is achieved[9]. Alternatively, a time-stepping method used in conjunction with some vortex-lattice[19] and panel[20] methods convects the shed vortex filaments with the instantaneous local velocity. This method is suited for unsteady flow problems, whereas the spacial wake-relaxation method assumes steady-state conditions exists. Still another scheme treats the wake as an array of two-dimensional point vortices moving in planes perpendicular to the free-stream velocity[21]. Precise analysis of deforming vortex sheets has been attempted recently and it has been noted that even for a simple two-dimensional vortex sheet problem, the calculation of the self-induced motion of vortex sheets is extremely difficult[22]. Based on these findings, it should be noted that the calculated shape of the deformed wake, regardless of the method used, may vary somewhat from reality. If near wake methods are used to calculate the induced drag, however, then the impact due to any differences between the calculated and the actual wake shapes will be greatly reduced.

IV. The Development of a Method for the Aerodynamic Design and Analysis of Planar and Non-Planar Wings

After considering the methods described, it was concluded that none had both the speed and accuracy required to be effective as a tool for designing wings having minimum overall drag. Thus, a hybrid method was created to take advantage of the best features of two of the methods. This method combines the lift distribution determination and the wake relaxation methodology of a low-order panel method with the induced drag calculation of the modified lifting-line method. The method is reasonably fast and retains sufficient accuracy to be useful for design work.

Panel Method Solution

The first element of the hybrid method is a low-order panel method which models the wing with flat panels each having a constant distributed source and doublet strengths. The wing wake is formed using vorticity filaments which are shed from a given point on the trailing edge. The strength of these filaments is taken as the difference in doublet strengths of the upper and lower surface panels which join to form the trailing edge at that point.

The determination of the lift and induced drag distributions about a wing in the presence of a free-wake begins by prescribing the wake to be in the same plane as the free stream velocity. The panel method is used to find the vorticity distribution on the wing and shed into the wake, as well as the velocities induced around the wing. Using this information, the trailing vortex filaments are relaxed to align themselves with the local velocities that have been determined in the wake. This wake relaxation is an iterative process and typically converges within about three iterations.

Once a new wake shape has been determined, the induced drag can be calculated with a method to be described shortly. Using the deformed wake shape, the panel method is again used to obtain vorticity and induced velocity values that are different from those obtained with the undeformed wake because the boundary conditions are no longer the same. With the new vorticity and induced velocities, the wake can be further relaxed toward a converged shape, and the induced drag recalculated. This procedure is continued until convergence, based on the change of the induced drag calculation from one iteration to the next, is achieved. Because the relaxed wake shape is much closer to the physical wake than one aligned with the free stream, the mutual interaction between the wing and the wake is more accurately modeled. Consequently, as this interaction influences the relationship between wing geometry and induced drag, the hybrid free-wake method should be beneficial in the design of wings having minimum drag.

Induced Drag Calculation

The induced drag is calculated in the hybrid method by application of the Kutta-Joukowski law,

$$\vec{F} = (\vec{V} \, x \, \vec{\Gamma})\rho$$

at the trailing edge of the wing. The induced drag is the streamwise component of the force per unit span vector. The velocity vector is that resulting from the free-stream velocity plus that induced by the trailing vortex filaments. The influence of the bound vorticity, that is, the velocity induced by the source and doublet distributions on the wing, is excluded in the determination of the velocity vector. This exclusion is an extension of the assertion by Munk[5] that the bound vorticity need not be included in the calculation of induced downwash because the influence from the transverse vortices of any two lifting elements is reciprocal and canceling. Although Munk's formulation was developed assuming a fixed wake, the influence of the bound vorticity is unaffected by what occurs downstream, and therefore this assertion should be equally valid whether the wake is fixed or free to deform. The shapes of the trailing vortex filaments needed for the calculation of the downwash velocity are obtained by placing the filaments along the velocity vectors that are found during the panel method solution. After the induced drag is calculated, the panel method is again used and, with the new wake shape, a new value for the induced drag calculated. This process is continued until convergence, based on the change in the calculated induced drag from one iteration to the next, is achieved.

It is of interest that the hybrid method originally made use of the panel method to calculate lift distributions, and the modified lifting-line method to determine the relaxed wake shape in addition to computing the induced drag. It was found, however, that while the modified lifting-line method yielded induced drag predictions that were very close to those of the hybrid method, the wake shapes that corresponded to these calculations were very different. In retrospect, this is understandable in that, unlike in the case of the hybrid method, the modified lifting line method ignores any chordwise influences on the near-wake rolling-up process and, consequently, the converged wake geometries are very different. Because of this, the wake relaxation in the hybrid scheme is now performed in the panel method part of the program.

Extrapolation Factor

An important element of the present method is an extrapolation factor which largely eliminates the dependence of the computed induced drag on the spanwise number of panels used in modeling the wing. This factor is a function of the number of spanwise panels and is calculated by comparing the induced drag computed using the modified lifting-line part of the hybrid method with a fixed wake to that determined analytically for an elliptically loaded wing. Specifically, the extrapolation factor is found by applying the Kutta-Joukowski law at the trailing edge of an elliptically loaded wing using the velocity induced by a flat, fixed wake modeled with a given number of trailing vortex filaments. The strengths of the trailing filaments are equal to the spanwise derivative of the bound vorticity. As the span efficiency for this case is known analytically to be unity, the ratio of this with the span efficiency computed by the above method can be used as an extrapolation factor for any results computed using the same number of spanwise increments. As will be shown in the next section, the extrapolation factor dramatically reduces the number of spanwise wing panels needed to accurately determine the induced drag and significantly reduces the computational requirements.

V. Validation Using Computed Results

Because many of the difficulties in predicting induced drag using theoretical methods also extend to experimental determinations, the validation of the hybrid panel/trailing-edge method must rely largely on testing its robustness, evaluating its self-consistently, and comparing results obtained using it to those of other computational methods.

The wings used in the validation exercises, shown in Fig. 1, all have elliptical chord distributions and aspect ratios of 7.0. The location of the trailing edge of the wing geometries is given by

$$x_{te} = c_{root}\left[\left(\frac{x_{tip}}{c_{root}}\right)\left(1 - \sqrt{1 - \eta^2}\right) + \sqrt{1 - \eta^2}\right]$$

where η is the non-dimensional span location, and the tip location (x_{tip}) relative to the root chord varies from $0.25c_{root}$ to $1.50c_{root}$. The airfoil section used on all of the wings is the NACA 0012. Although the hybrid code can analyze models with both twist and dihedral, neither was included in the validation test runs.

Extrapolation Factor

The extrapolation factor discussed in the previous section is presented as a function of the number of spanwise increments in Fig. 2. Fig. 3 shows the advantage of using the extrapolation factor by plotting the calculated value of the span efficiency factor, e, against the relative tip location for constant chordwise but different spanwise panelling densities. Without the use of the extrapolation factor, e varies significantly as a function of the spanwise panelling density as is shown by the uncorrected curves. For spanwise panel densities of greater than 20, however, e is essentially independent of panelling density when use is made of the extrapolation factor. This result will be further demonstrated by comparison to a higher order panel method in the following sections.

As demonstrated in Fig. 4, the value of e is seen to be relatively insensitive to the number of chordwise panels, provided at least 50 panels (25 upper surface, 25 lower surface) are used.

Comparison with the Results of Other Computational Methods

To further test the validity of the hybrid panel/trailing-edge method, results have been compared to those obtained from it. A brief description of these methods follows.

Pressure Integration

The most direct way to predict induced drag using a panel method is to sum the streamwise components of the predicted surface pressure forces over all of the wing panels. Since the mathematical model used does not account for viscous effects, the streamwise force thus computed is the induced drag. It has been shown that the induced drag calculated in this way is extremely sensitive to the panel density in both the spanwise and chordwise directions[2,3]. Thus, the major shortcoming of this prediction method is that to obtain reasonably consistent results, a large number of surface panels must be used and the required computational time becomes prohibitive, especially for design purposes.

Another problem associated with the use of pressure integration is due to numerical round-off which results in "leakage" because the source contributions of all the panels do not sum exactly to zero. Thus, it is found that a small amount of lift, and consequently induced drag, is predicted when the wings are operated at zero angle of attack. Since the wings are untwisted and the airfoil symmetric, this is clearly in error and, although small, must be taken into account. Fig. 5 shows the dependence of this error on the tip location and the panel density for the low-order panel method used in the present study, and compares this to a similar error obtained using a higher-order method and presented in Ref. 3. The error in the zero-lift drag prediction appears to depend on the tip location; however, increasing the number of spanwise panels causes this dependence to disappear. This behavior is corroborated by the results of Ref. 3. With 100 chordwise by 10 spanwise (100x10) panels, the error with rearward tip location is very similar to that of the hybrid method. As the panel density is increased to 100x50, however, the error is essentially independent of the tip location. Thus, for a given number of chordwise panels, increasing the spanwise panel density causes the zero-lift error to approach that of the tip location at .25c. Consequently, a correction based on the zero-sweep error for a given chordwise density can be applied to the pressure integration induced drag calculations. In the test cases that follow, the pressure integration results are presented both with and without the inclusion of a correction for the zero-lift error. These two extremes are presented as an upper and lower bound on the pressure integration results.

Finally, it should be noted that the pressure integration results presented do include an effect from the deforming wake. This comes about in the computation of the pressure on the wing surface by including the contribution of velocity induced by the deformed wake.

Trefftz-Plane Method

Following the formulation by Trefftz[23], the induced drag is computed assuming the wake to be fixed and aligned with the free-stream velocity. The Trefftz method used here differs from the hybrid panel/trailing-edge method only in that the wake is undeformed. In the following comparisons, the difference in results between the hybrid method and the Trefftz method can be taken to be the influence of the freely deforming wake.

Modified Lifting Line

The last method used for comparison employs the modified lifting-line calculation of induced drag[7]. This method takes the spanwise circulation distribution predicted by the low-order panel method, computes the corresponding strength of the trailing streamwise vortex filaments shed into the wake, then relaxes the wake using only the influence of the trailing wake vortices. The induced drag is then computed by applying the Kutta-Joukowski law at the wing trailing edge using the velocity induced by the deformed wake and the wing circulation assumed to be concentrated at the trailing edge. Unlike the hybrid method, the modified lifting-line method does not include any influence from the bound vorticity on the wing in calculating the shape of the deformed wake.

Comparison of Results

For an angle of attack of 4 degrees, the span efficiency factor, e, as calculated using pressure integration, Trefftz-plane method, modified lifting-line method, and the hybrid panel/trailing-edge method, is presented as a function of tip location in Fig. 6. The methods all use a panelling density of 50 chordwise, where appropriate, and 20 spanwise (half-span) panels. By comparing the hybrid method with the Trefftz-plane method, it is observed that wake roll-up causes a performance penalty, but that this penalty decreases with more aft tip locations. Finally, it should be noted that for this case, the difference between the corrected and uncorrected pressure integration calculations would result in a variation of $\pm.0003$ in the induced drag coefficient calculation. As this variation is much larger than the differences due to planform shape predicted by any of the other methods, the value of pressure integration methods not having very large panelling densities is again called into question. Results similar to the preceding figure, but for an angle of attack of 8 degrees, are presented in Fig. 7.

The hybrid panel/trailing-edge method and the similar Trefftz-plane method show the most consistency between the 4 and 8 degree angle of attack cases, as the other methods show a reversal in their predicted trends. Although it is expected that e will change slightly with angle of attack, the trend reversals predicted by the other methods do not seem very likely. The consistency of the hybrid method suggests that it is less prone to error at higher angles of attack than the other methods, especially pressure integration, and is therefore more robust. The reduction in induced drag with moving the tip location aft corresponds to recent experimental results[24], and has been predicted by others using various methods over the past several years[1-3]. Clearly, however, because all of the inviscid predictions ignore the vortex that would form in the region of the highly swept tip, the benefits indicated with the very far aft tip locations are not likely to be realized.

In Fig. 8, the span efficiency predictions of the present method are compared with those of the higher-order panel method of Ref. 3. This method uses pressure integration for the induced drag calculation and requires 100 chordwise and 70 spanwise panels to approach a consistent result. In contrast, the hybrid panel/trailing-edge method essentially matches those results with only 50x20 panels. If it is assumed that the computation time of the panel methods vary with N^2, the hybrid method will run approximately 50 *times faster* than the higher-order panel method for the same level of accuracy.

VI. Validation Using Experimental Results

Description of Test Models

In addition to comparing results to other theoretical methods, validation studies were undertaken for the hybrid panel/trailing edge method by comparing its predictions against experimental results. The experimental data used are those obtained from wind-tunnel tests at the NASA Langley Research Center. The wing geometries used for this comparison are similar to those used in the computational validation of the previous section. Each wing has an elliptical chord distribution with varying tip locations. The location of the quarter chord point at each spanwise station is defined by the position of the wing tip relative to the root chord and is given by the expression

$$x_{.25c} = c_r\left(\frac{x_{tip}}{c_r}\right)\left(1 - \frac{3}{4}\frac{c}{c_r}\right).$$

The wings used in the wind-tunnel tests have tip locations at 0.25 (unswept elliptical), 1.50 (crescent shaped), and 1.00 (straight trailing-edge) relative to the root chord. An NLF(1)-0416 airfoil section[25] is used on each model, and the transition point fixed by trip strips at 7.5% chord. The wings of the wind-tunnel models are untwisted, have a span of 48.0 inches, a projected area of 384.0 sq.in., and an aspect ratio of 6.0. Each of the wings is mounted on a common 3.0 inch diameter center body. The influence of the centerbody is not included in the computational predictions. The geometries of these wings (without the centerbody) are shown in Fig. 9.

Prediction Method

The hybrid panel/trailing-edge method was used to predict the inviscid (vortex) induced drag of the experimental wings. The wings were modeled with 60 chordwise (30 upper, 30 lower) panels and 20 spanwise (half-span) panels. The span efficiency factor was obtained using the same procedure as described in the previous sections.

The profile drag of the models was built-up using a strip analysis with the section lift coefficients predicted by the panel method. The section profile drag coefficients of the NLF(1)-0416 airfoil as a function of chord Reynolds number and section lift coefficient were obtained using the airfoil design and analysis program of Ref. 26. The effects of flow separation at the higher lift coefficient are not taken into account.

Presentation and Discussion of Results

The results from the wind-tunnel tests and the predictions of the hybrid panel/trailing-edge method are presented in Figs. 10-21, and in Table 1. Comparisons between the experimentally measured and the predicted performance for each wing are presented in Figs. 10-12. The drag is slightly overpredicted at low lift coefficients in all cases and underpredicted at high lift coefficients for the crescent-shaped wing. The change in drag with respect to lift is predicted fairly well up to moderate lift coefficients for all of the wings. Figs. 13 and 14 can be used to compare the performance of the wings relative to one another as measured experimentally and as predicted by the hybrid method. The predicted results agree with the measured data in that the straight trailing-edge wing exhibits a drag lower than the unswept elliptical wing even to high lift coefficients. As expected, however, the prediction method does not capture the significant increase in drag for the crescent-shaped wing at high lift coefficients because the inviscid method does not account for the separated flow that occurs over the tips of the highly crescent planform.

The measured and the predicted drag coefficients are presented in Figs. 15-19 as a function of C_L^2, from which Oswald efficiency factors can be determined. The measured data in Figs. 15-17 show that the Oswald efficiency for each of the three wings is not constant over the range of lift coefficients for which they were tested. As expected, due to flow separation, the measured Oswald efficiency decreases with increasing lift coefficient. The change is greatest for the crescent-shaped wing. In the case of the unswept elliptical and straight-trailing-edge wings, the predicted Oswald efficiency matches the measured efficiency over the C_L range from approximately 0.7 to 0.9. For the crescent-shaped wing, the predicted and measured Oswald efficiencies match for lift coefficients from 0.6 to 0.8. In all cases, the hybrid method underpredicts the Oswald efficiency at low C_L and overpredicts it at high C_L.

In Figs. 18 and 19, it can be seen that the experimental and predicted results agree in that both show the relative inferiority of the unswept elliptical wing. Based on these data and the theoretical results of the following sections (see Fig. 25), this result is probably due to the deviation of the spanwise lift distribution from elliptical. Above a lift coefficient of 0.7, the experiment shows the crescent-shaped wing to be clearly inferior to the straight-trailing-edge wing. This is likely due to flow separation on the highly swept tips of the crescent-shaped wing as observed in flow visualization studies during the experiment.

Obviously this viscous effect is not captured in the inviscid prediction method and, in fact, the predicted results actually show the straight-trailing-edge wing slightly inferior to the crescent wing above a lift coefficient of 0.7. This discrepancy results from the error in the predicted profile drag component which is added to the hybrid method inviscid induced drag prediction. To illustrate this, the predicted *inviscid* induced drag coefficient is presented as a function of C_L^2 in Fig. 20. It can be seen that the crescent-shaped and straight-trailing-edge wings have nearly identical span efficiencies, with the unswept elliptical wing being clearly inferior.

As a means of separating the effects of the viscous and the inviscid drag components at lift coefficients between 0 and 0.7, Fig. 21 presents a comparison between the measured (total) drag coefficient and the predicted vortex (inviscid) induced drag coefficient both as functions of C_L^2. The predicted curves have been offset by a constant amount to aid in comparing their slopes to those of the measured data. It can be seen in this figure that for the unswept elliptical wing the measured Oswald efficiency matches the predicted span efficiency over this entire range of lift coefficients. For the other two wings, the drag due to lift analysis must be separated into moderate and low lift coefficient ranges. In the moderate C_L range (0.4 to 0.7) the measured drag due to lift of the crescent-shaped wing becomes dominated by the drag increase due to flow separation at the tips. This is illustrated in Fig. 21 by the departure of the measured drag from the linear C_D vs. C_L^2 relationship above a lift coefficient of 0.5. In the low C_L range (0 to 0.4) the measured data of the straight-trailing-edge wing has the most pronounced departure from the linear C_D vs. C_L^2 relationship. It is believed that this wing takes advantage of the decreasing section profile drag of the airfoil as lift is increased from $C_L = 0$ to $C_L = 0.4$ without experiencing the detrimental effects of wake roll-up as experienced by the unswept elliptical wing, or the tip flow separation experienced by the crescent-shaped wing. The straight-trailing-edge wing actually attains a measured Oswald efficiency greater than unity in the lift coefficient range between 0 and 0.7. The measured and predicted Oswald efficiencies over the C_L range of 0 to 0.7, and the predicted span efficiency over the entire C_L range are presented in Table 1.

VII. Discussion of Tools for the Design of Planar and Non-Planar Wings Having Minimum Induced Drag

In order to design wings having minimum induced drag, it is necessary to know the optimum lift distribution in the presence of the freely deforming wake. Using the lifting-line model, Munk concluded that for the induced drag of a wing to be a minimum, the induced downwash at the lifting line must be constant if the wing is planar, or given by the relation

$$\omega_i = \omega_o \cos\theta$$

where ω_o is a constant and θ the local dihedral angle, if the wing is non-planar[5]. Although Munk assumed that the wake was non-deforming, the reasoning leading to the above conclusion does not depend upon the mechanism which generates the downwash. In determining the spanwise lift distribution which generates the optimum downwash distribution, the assumption of the fixed wake does become important. The classical result of the optimum elliptic lift distribution follows immediately if this assumption is made. The question that remains, however, is what lift distribution generates the optimum downwash distribution for minimum induced drag in the presence of free wake. As no mathematical solution to this question is as yet available, a first step in addressing it was taken when, in the course of this research, it was shown that for a straight lifting line with an elliptical lift distribution the induced drag is independent of wake rollup. Given this result and in lieu of a complete mathematical proof, it is assumed that the free wake does not significantly alter Munk's result concerning the optimal lift distribution for the minimization of induced drag. To test this assumption, the induced drag was calculated using the modified lifting-line method with an optimal lift distribution prescribed according to Munk's result. The induced drag was then calculated with the lift distribution slightly perturbed from the prescribed optimum. In all cases considered, the drag increased. Thus, for the present time, even if the Munk result is not truly optimal, it is considered to be close enough for engineering purposes.

The effect of the deforming wake on the spanwise lift distribution of three wings with elliptical chord distributions is shown in Figs. 22-24 which present the *error* in the spanwise lift distribution from the optimum. It can be seen that the deforming wake has the largest effect on the wing with the tip at 0.25 root chord (straight quarter-chord line). As the tip location is moved aft, the wake deformation has less and less effect on the lift distribution. This is demonstrated in Fig. 23 for the straight-trailing-edge wing and in Fig. 24 for the crescent shaped wing. It is suggested that the aft-located tip isolates the rolled wake from the rest of the wing and, consequently, decreases its influence. These results are combined and presented in Fig. 25 where it can be seen that the straight-trailing-edge wing maintains the closest to optimal lift distribution, particularly near the tip. It is interesting to note, that even though the lift distribution of the crescent-shaped wing is farther from elliptical than the straight-trailing-edge wing, the results presented in the previous section predict the crescent-shaped wing to have slightly higher span efficiency. Some part of this effect is that the benefit of moving the wake aft more than offsets the penalty of the lift distribution not being elliptical. A more significant contribution to this effect, however, is that because the panel method predicts negative lift at the tip, application of the Kutta-Joukowski law here results in a small amount of "induced thrust," overcoming the deficiency of the non-optimum lift distribution. This effect is very small and certainly nullified by viscous effects in the real flow. This conclusion is supported by the previously presented experimental results.

Preliminary results of using the hybrid panel/trailing-edge method for the design of a non-planar wing having minimum induced drag is illustrated in Fig. 26. At the top of this figure, the lift distribution error from optimum is plotted against span for an arbitrary (starting) wing planform and winglet geometry. In this case, the wing under consideration has winglets which are 0.1 semi-span in height. Based on the error, the chord was adjusted appropriately in the locations where it is over or under that needed for the optimum lift distribution. As shown in the other two graphs, the lift distributions for the second and third geometry iterations are closer to optimum. While these iterations are presented only to demonstrate the potential, it is clear that this process can be continued until convergence to the optimum span lift distribution is achieved. The same optimization procedure can be applied to any non-planar geometries with different dihedral distributions or winglet configurations and their overall performance compared. In this way, the hybrid method provides a valuable tool for the design of a mission specific, optimum non-planar wings.

VIII. Conclusions and Recommendations

The newly developed hybrid panel/trailing-edge method is a valuable tool for taking the non-linear effects of a freely deforming wake into account in determining the induced drag of planar and non-planar wing geometries. When compared to other methods, it is found that it achieves equivalent accuracy with considerably less computational time. Given its speed and robustness, the hybrid method should prove most useful in the design of planar and non-planar wings having minimum induced drag.

Using the hybrid panel/trailing-edge method, the influence of planform geometry on the induced drag of planar wings has been explored. It is found that the benefit of crescent-shaped planforms for reducing induced drag that has been noted by others is confirmed; however, this benefit is not nearly as great as has sometimes been suggested. For the family of wings considered, the reduction in induced drag that is possible for a wing operating at a lift coefficient of 1.0 and having a straight trailing edge, as compared to one having no sweep, is approximately 1%. For any further aft tip geometries, the additional reduction in induced drag is not significant and certainly not enough to offset the unaccounted for penalties due to viscous effects that would accompany the more crescent planforms.

In exploring the effect of the freely deforming wake on the wing lift distribution, it is found that the free wake has a significant influence on the lift distribution of the unswept elliptical wing, but that this effect is diminished when the tip is moved aft. Once the tip is located such that the wing has a straight trailing edge, any further aft movement seems to have little effect on the lift distribution and, consequently, on the span efficiency.

While it seems that the impact of planform shape on reducing the induced drag of planar wings is limited, significant gains appear to be possible using non-planar wing configurations. While well-suited non-planar wing design methods have not been available, the speed and accuracy of the hybrid method make it ideal for this problem. Based on the few non-planar cases examined thus far, the method appears to handle these cases as well as it does planar ones. By combining the hybrid method for analyzing induced drag with methods that predict profile drag, wing geometries which have minimum overall drag can be designed.

At this point, it is recommended that the methods developed be used to design a wind-tunnel experiment to compare mission specific planar and non-planar wings. As there is no common basis of comparison otherwise, by designing an optimum planar and an optimum non-planar wing to the same mission requirements it is possible to determine if the gains promised by non-planar geometries are realizable. In addition, as quality experimental data for non-planar wings is non-existent, the results of such an experiment would be invaluable for the development and calibration of any non-planar wing analysis methods.

Finally, if the results of the recommended experiment support the promise that aerodynamic gains are possible using non-planar wing geometries, then it remains to develop a method that includes the effects of compressibility and allows a designer to trade-off these gains against other factors such as weight, wing-root bending moment, and so forth.

IX. References

1. Van Dam, C. P., "Induced-Drag Characteristics of Crescent-Moon-Shaped Wings," *Journal of Aircraft*, Vol. 24, No. 2, February 1987, pp. 115-119.

2. Kroo, I. and Smith, S. C., "The Computation of Induced Drag with Nonplanar and Deformed Wakes," SAE 901933, SAE Aerospace Technology Conference and Exposition, October 1990.

3. DeHaan, M. A., "Induced Drag of Wings With Highly Swept and Tapered Wing Tips," AIAA-90-3062-CP," *AIAA 8th Applied Aerodynamics Conference, A Collection of Technical Papers*, August 1990, pp. 571-581.

4. Prandtl, L., "Applications of Modern Hydrodynamics to Aeroacoustics," NACA Report No. 116, 1921.

5. Munk, M. M., "The Minimum Induced Drag of Aerofoils," NACA Report No. 121, 1921.

6. Cone, C. D., Jr., "The Theory of Induced Lift and Minimum Induced Drag of Non-planar Lifting Systems," NASA TR R-139, 1962.

7. Eppler, R., "Die Entwicklung der Tragflugeltheorie," *Z. Flugwiss*, November 1987, pp. 133-144.

8. Falkner, V. M., "The Calculation of Aerodynamic Loading on Surfaces of Any Shape," ARC R & M 1910, 1943.

9. Butter, D. J. and Hancock, G. J., "A Numerical Method for Calculating the Trailing Vortex System behind a Swept Wing at Low Speed," *The Aeronautical Journal of the Royal Aeronautical Society*, Vol. 75, August 1971, pp. 564-568.

10. Schlichting, H. and Thomas, H.H.B.M,, "Note on the Calculation of the Lift Distribution of Swept Wings," R.A.E. Report No. AERO 2236, December 1947.

11. Robinson, A. and Laurmann, M. A., *Wing Theory*, Cambridge University Press, Cambridge, 1956.

12. Schlichting, H. and Truckenbrodt, E., *Aerodynamics of the Airplane*, McGraw-Hill, New York, 1979.

13. Jones, R. T. and Cohen, D., *High-Speed Wing Theory*, Princeton University Press, Princeton, 1960.

14. Katz, J. and Plotkin, A., *Low-Speed Aerodynamics*, McGraw-Hill, New York, 1991.

15. Maskew, B., "Prediction of Subsonic Aerodynamic Characteristics: A Case for Low-Order Panel Methods," *Journal of Aircraft*, Vol. 19, Feb. 1982, pp. 157-163.

16. Samant, S. S., Bussoleti, J. E., Johnson, F. T., Burkhart, R. H., Everson, B. L., Melvin, R. G., and Young, D. P., "TRANAIR: A Computer Code for Transonic Analysis of Arbitrary Configurations," AIAA Paper 87-0034, January 1987.

17. Van Dam, C. P., Nikfetrat, K., Vijgen, P.M.H.W., and Fremaux, C. M., "Calculation and Measurement of Induced Drag at Low Speeds," SAE 901935, SAE Aerospace Technology Conference and Exposition, October 1990.

18. Tinocco, E. N., "CFD Applications to Complex Configurations: A Survey," *Applied Computational Aerodynamics*, Henne, P. A. (ed.), *AIAA Progress in Aeronautics and Astronautics*, Washington, D. C., Vol. 125, Chapter 15, pp. 559-615.

19. Konstadinopoulos, P., Thrasher, D. F., Mook, D. T., Nayfeh, A. H., and Watson, L., "A Vortex-Lattice for General Unsteady Aerodynamics," *Journal of Aircraft*, Vol. 22, 1985, pp. 43-49.

20. Ashby, D. L., Dudley, M., Iguchi, S. K., "Development and Validation of an Advanced Low-Order Panel Method," NASA TM 101024, 1988.

21. Rossow, V. J., "Theoretical Study of Lift-Generated Vortex Wakes Designed to Avoid Rollup," *AIAA Journal*, Vol. 13, No. 4, 1975, pp. 476-484.

22. Higdon, J.J.L. and Pozrikidis, E., "The Self-Induced Motion of Vortex Sheets," *Journal of Fluid Mechanics*, Vol. 150, 1985, pp. 203-231.

23. Trefftz, E., "Prandtlshe Tragflachen und Propellertheorie," *Z. angew. Math. Mech.*, Vol. 1, 1921, p. 206.

24. Van Dam, C. P., Nikfetrat, K., Chang, I. C., and Vijgen, P.M.H.W., "Drag Calculations of Wings Using Euler Methods," AIAA-91-0338, AIAA 29th Aerospace Sciences Meeting, 1991.

25. Somers, D. M., "Design and Experimental Results for a Natural-Laminar-Flow Airfoil for General Aviation Applications," NASA TP 1861, 1981.

26. Eppler, R. and Somers, D. M., "A Computer Program for the Design and Analysis of Low-Speed Airfoils," NASA TM 80210, 1980.

Wing Geometry	Oswald's Efficiency Factor $0 < C_L < 0.7$		Span Efficiency Factor
	Measured	Predicted	Predicted
Unswept Elliptical	.9691	.9248	.9754
Crescent Shaped	.9800	.9463	.9866
Straight Trailing Edge	1.0102	.9381	.9823

Table 1: Measured and Predicted Efficiency Factors for the NASA LaRC Test Wings

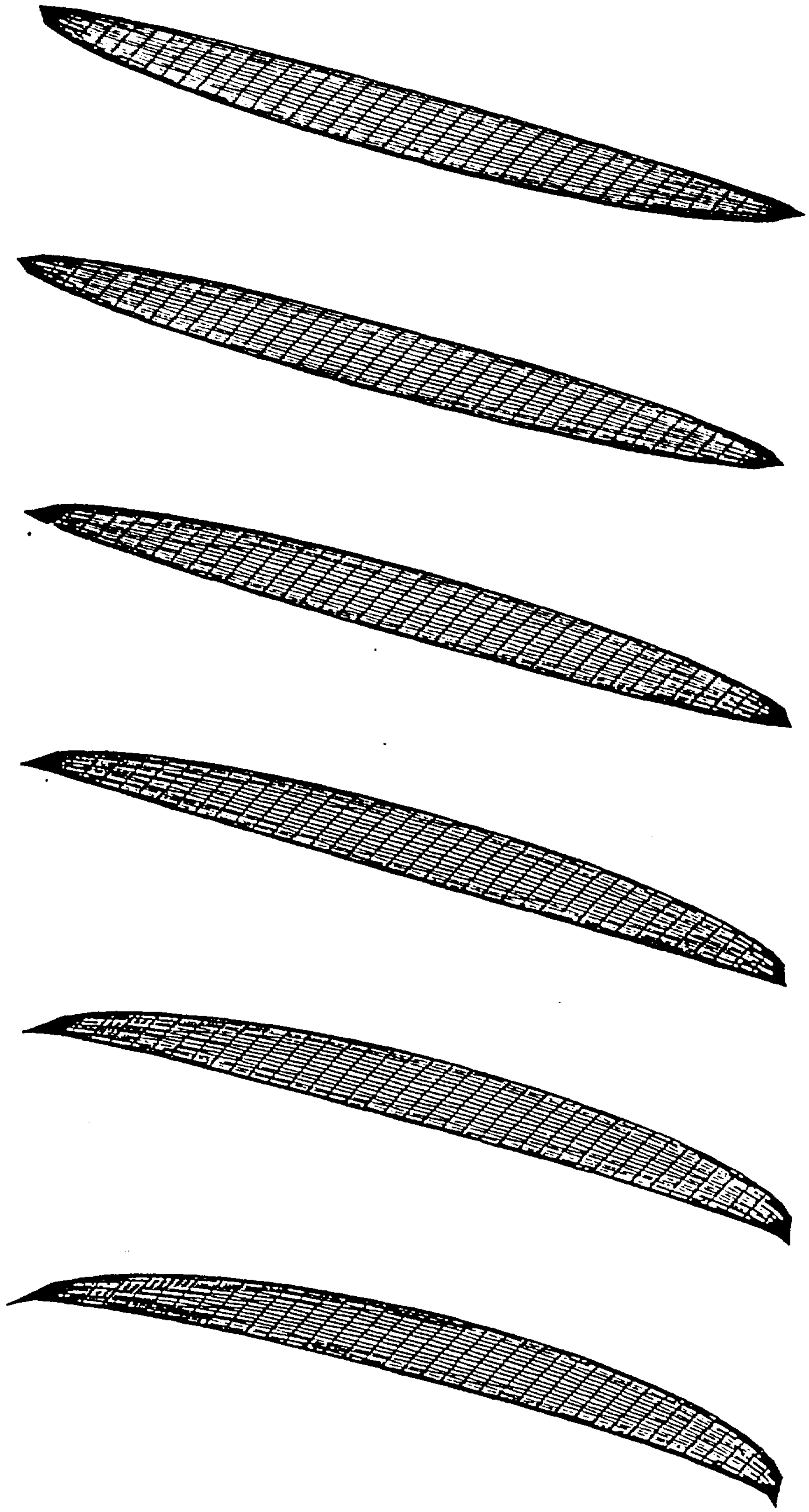

Figure 1: Wing Geometries Used for the Computational Validation of the Hybrid Panel/Trailing-Edge Method from Unswept Elliptical Wing (top) to Full Crescent-Shaped Wing (bottom).

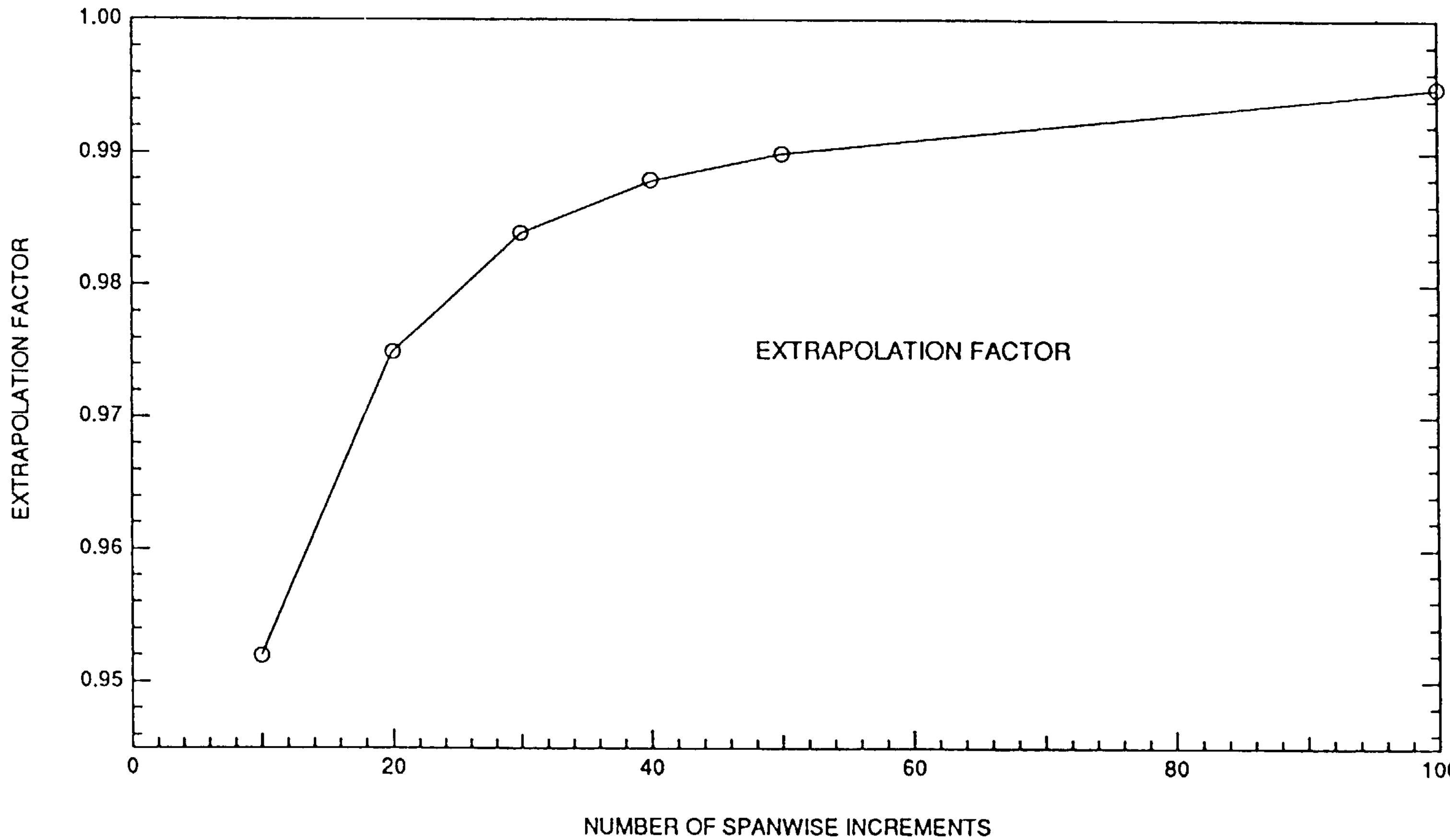

Figure 2: Extrapolation Factor for Hybrid Panel/Trailing-Edge Method

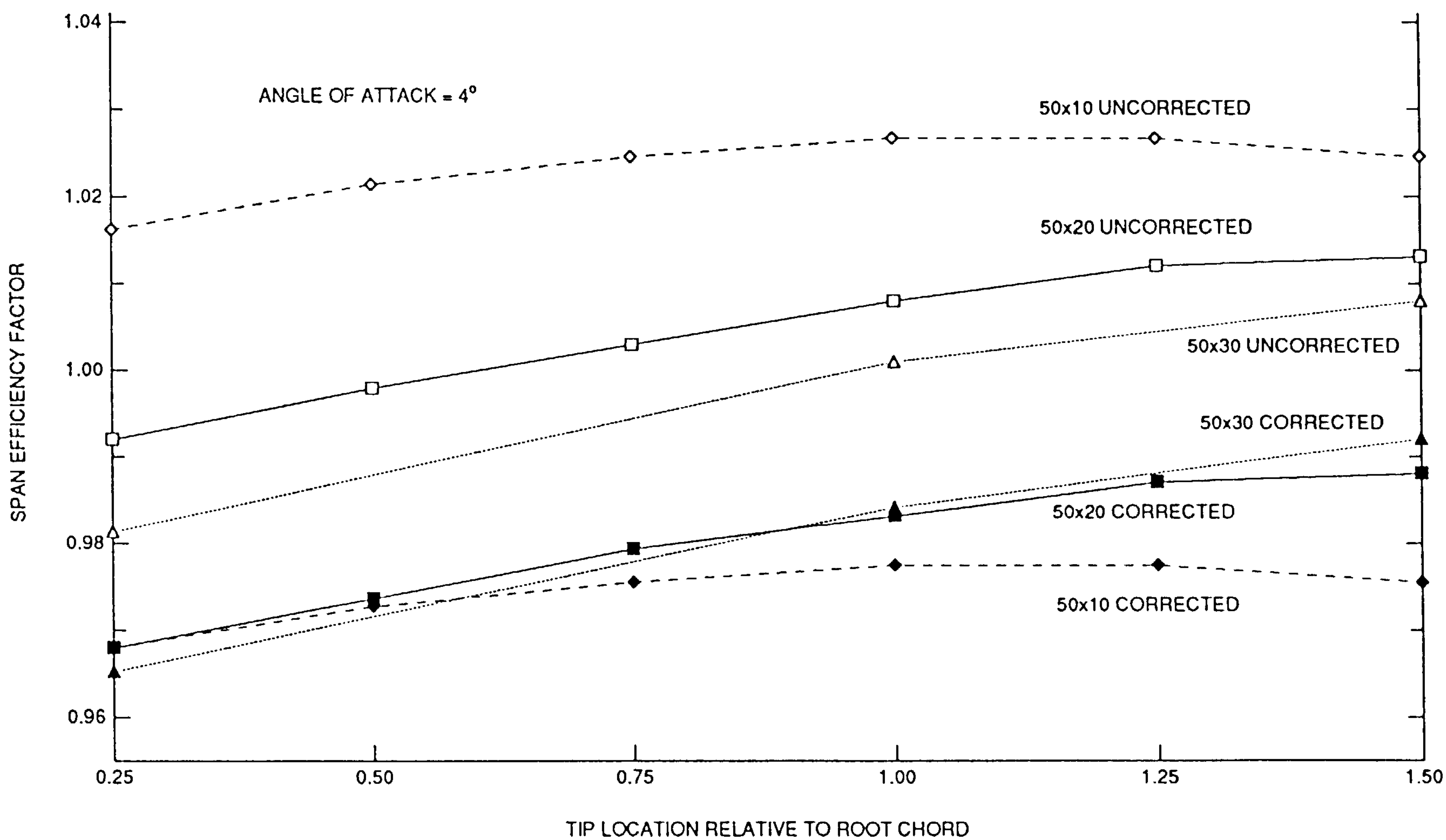

Figure 3: Effect of Extrapolation Factor Correction on Results from the Hybrid Panel/Trailing-Edge Method, 4 degrees Angle of Attack

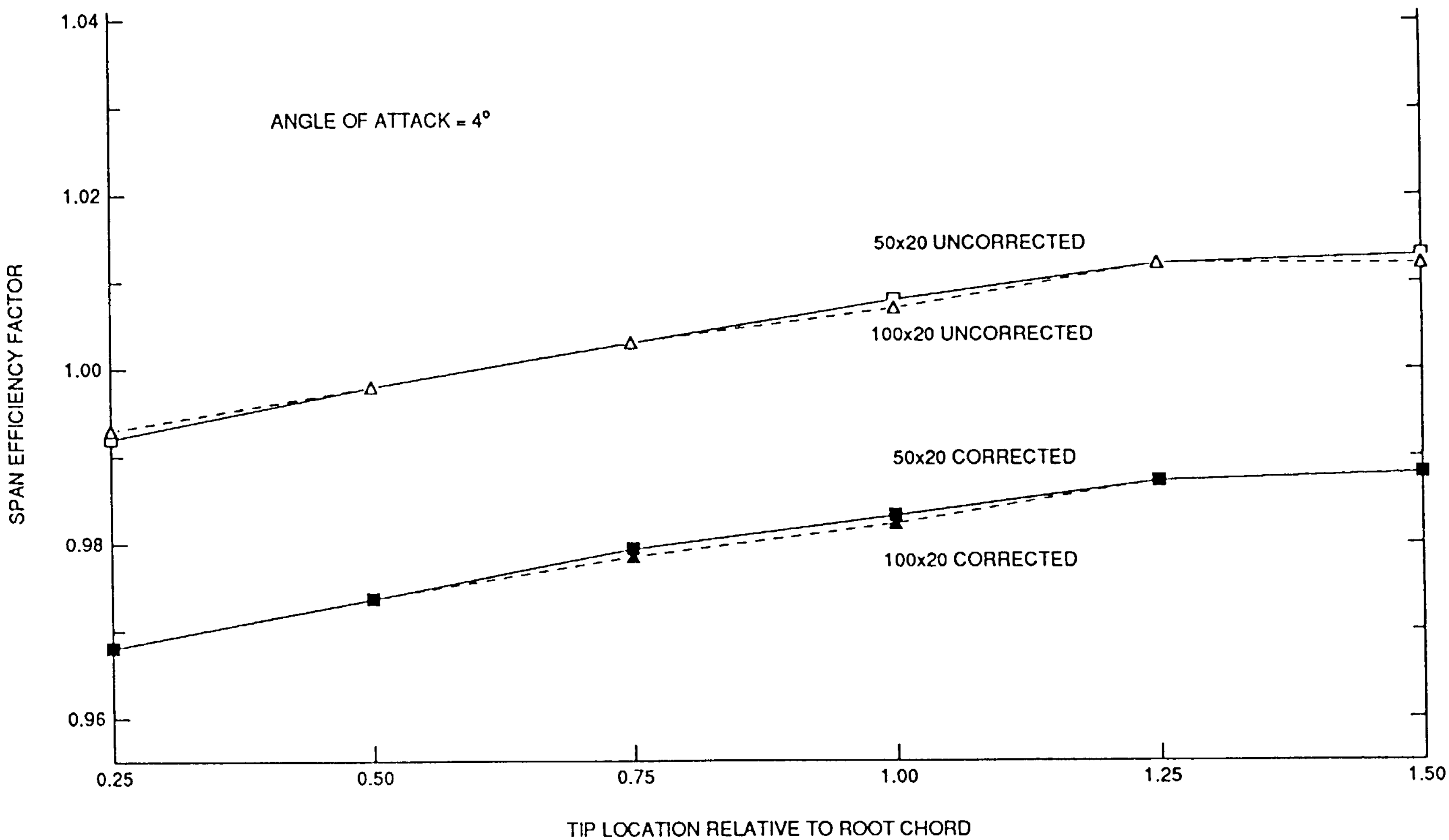

Figure 4: Dependence of Span Efficiency Factor on Chordwise Panel Spacing , 4 degrees Angle of Attack

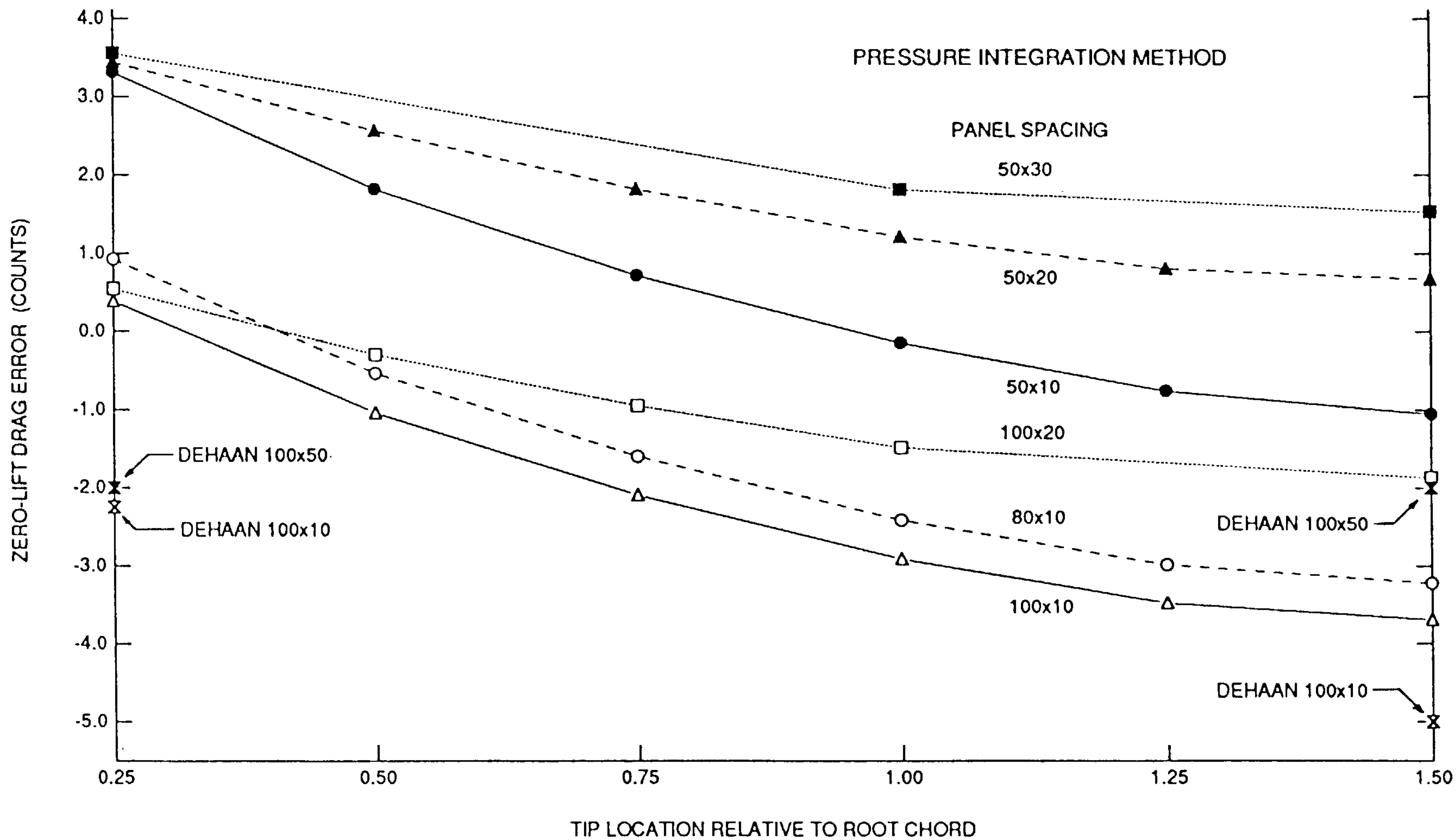

Figure 5: Pressure Integration Method Zero-Lift Drag Error

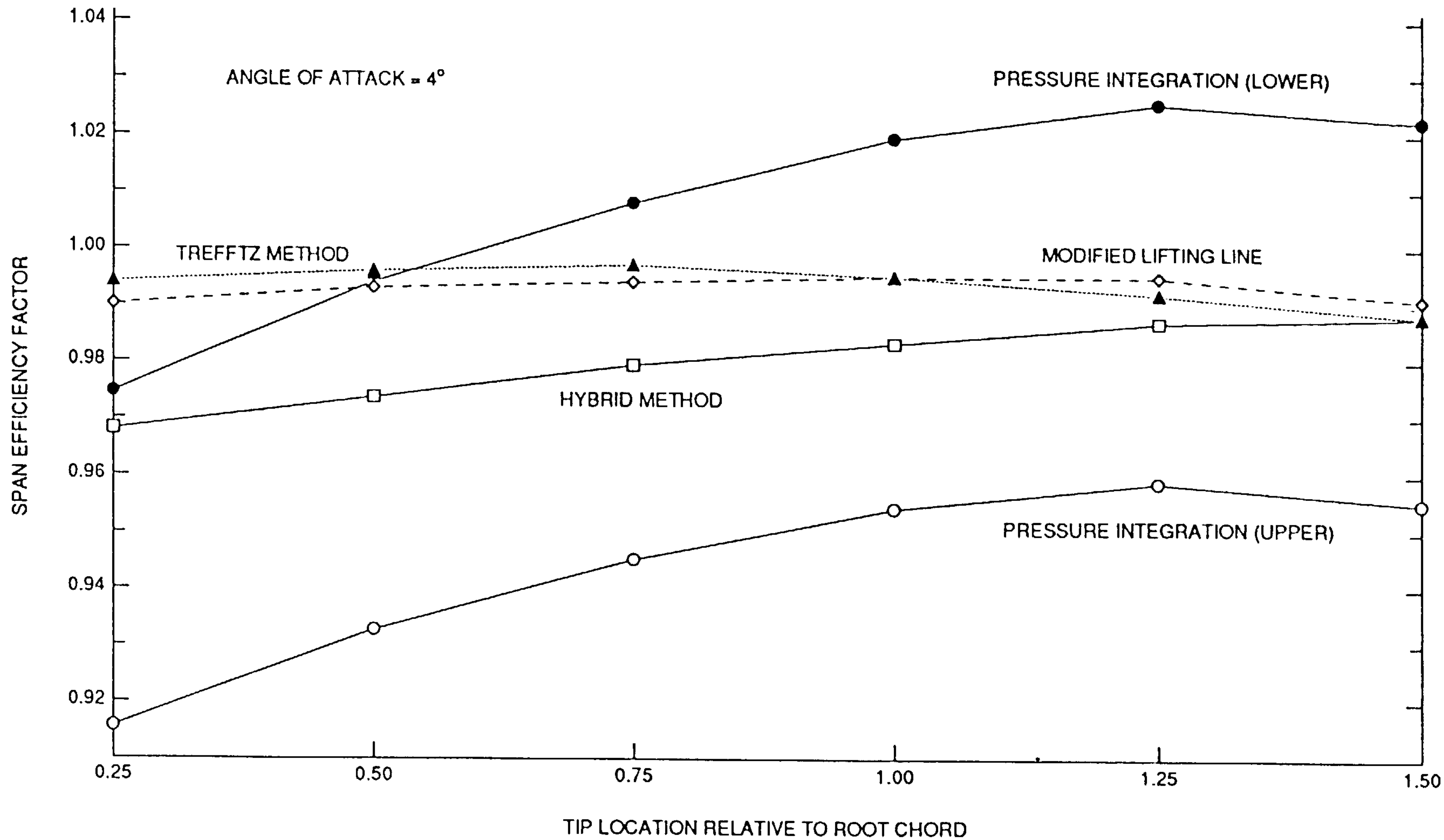

Figure 6: Comparison of Induced Drag Prediction Methods, 4 degrees Angle of Attack

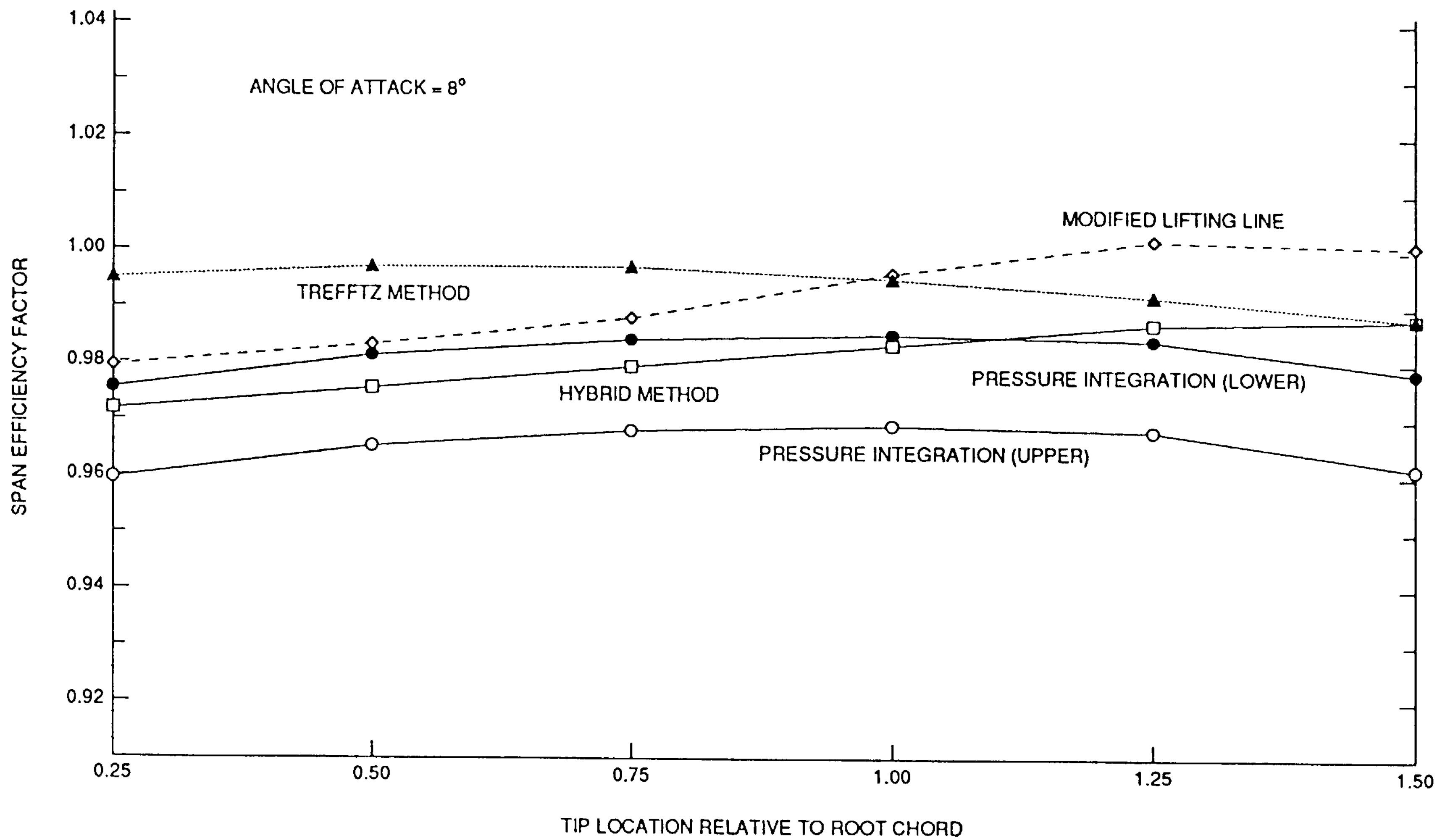

Figure 7: Comparison of Induced Drag Prediction Methods, 8 degrees Angle of Attack

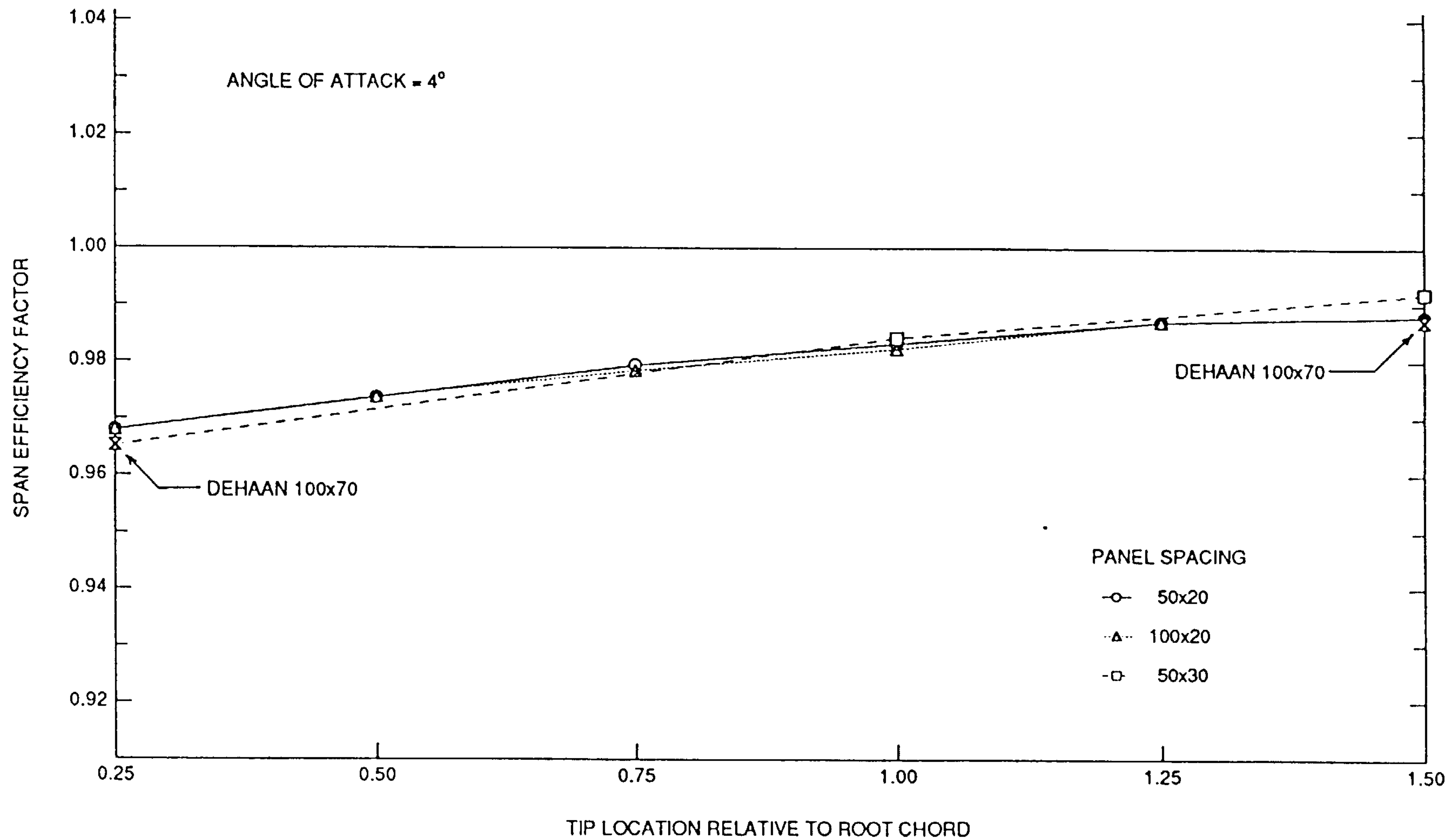

Figure 8: Comparison of Results between the Hybrid Panel/Trailing-Edge Method and a Higher-Order Panel Method

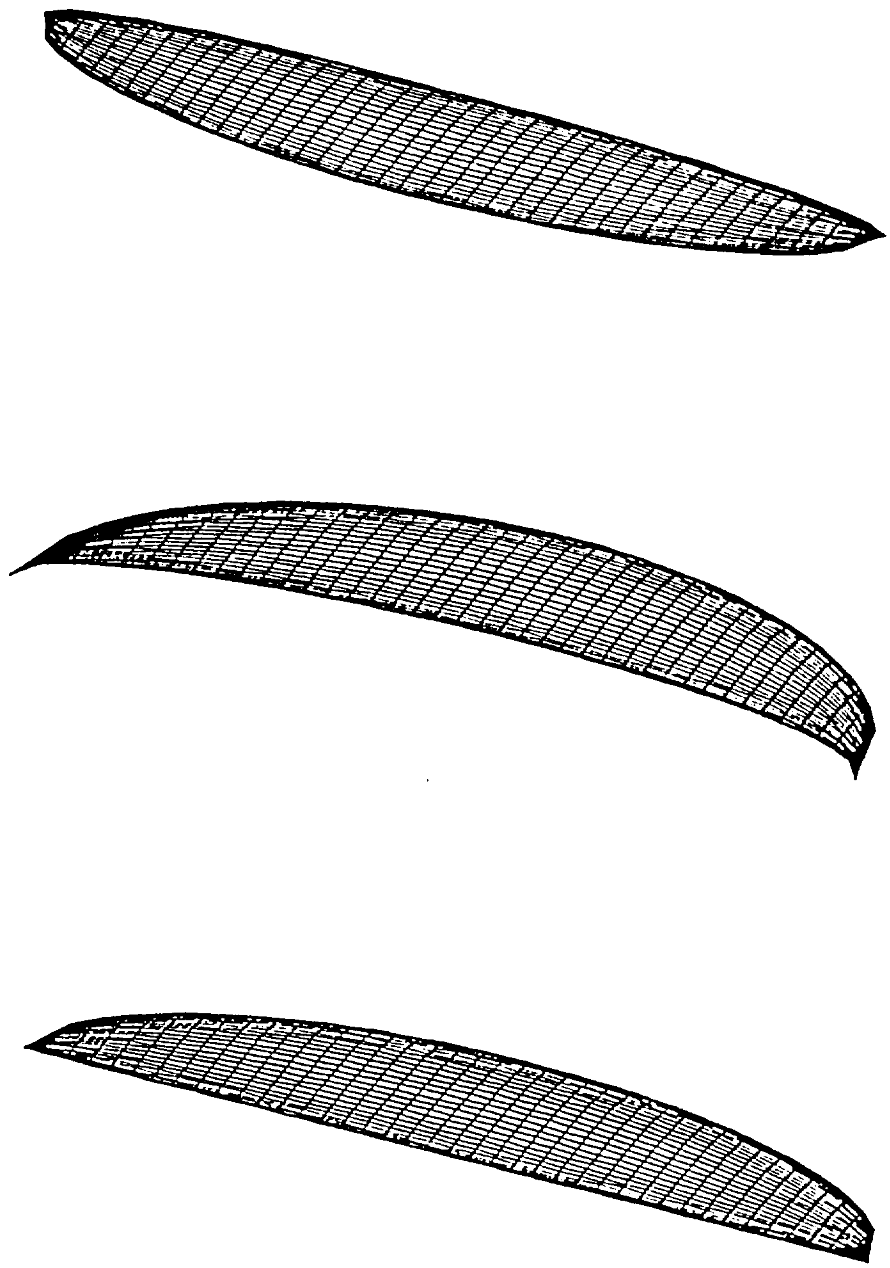

Figure 9: Wing Geometries Used for the Experimental Validation of the Hybrid Panel/Trailing-Edge Method; Unswept Elliptical (top), Crescent-Shaped (center), and Straight Trailing-Edge (bottom)

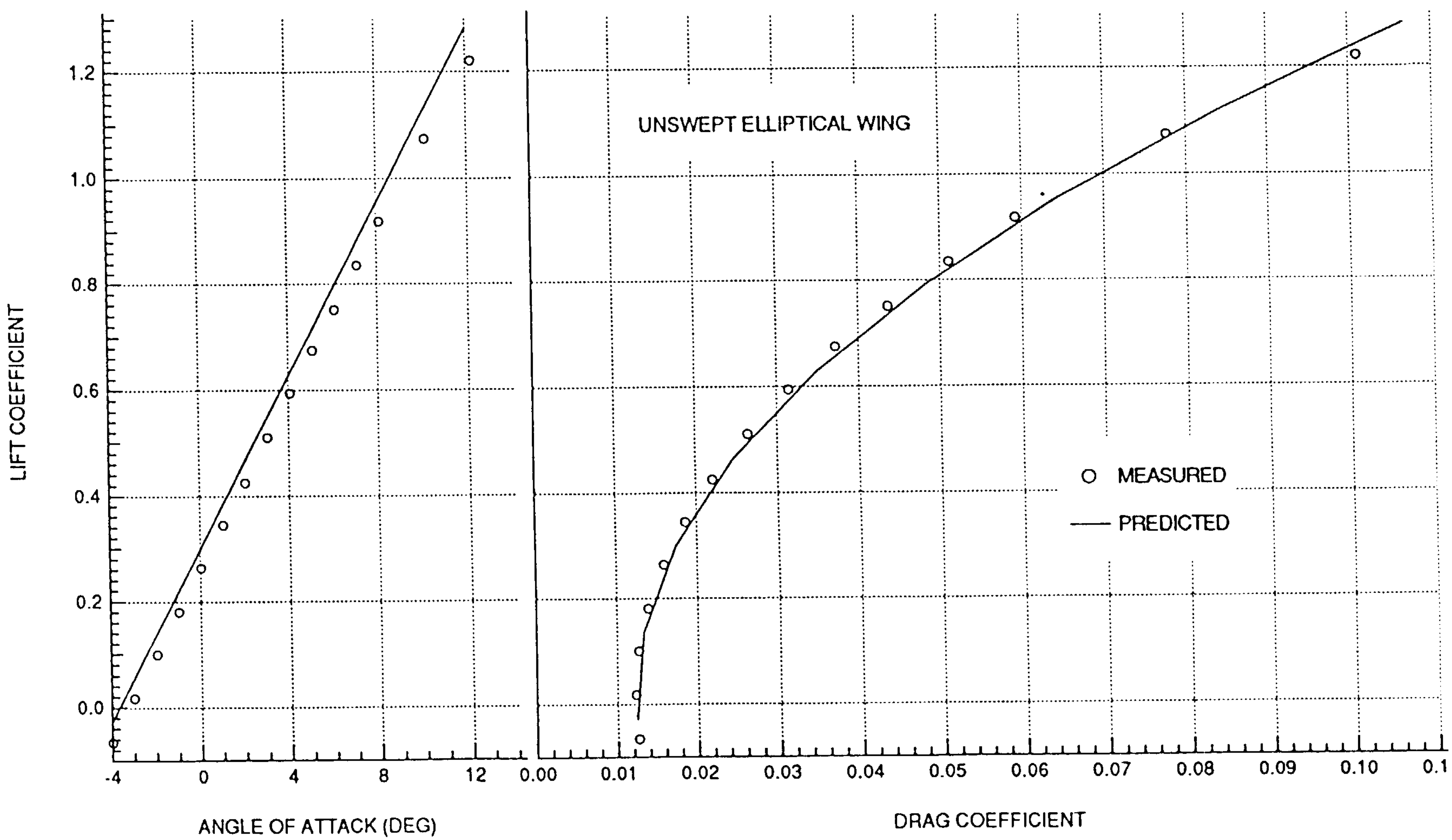

Figure 10: Comparison of the Measured and Predicted Lift and Drag of the Unswept Elliptical Wing

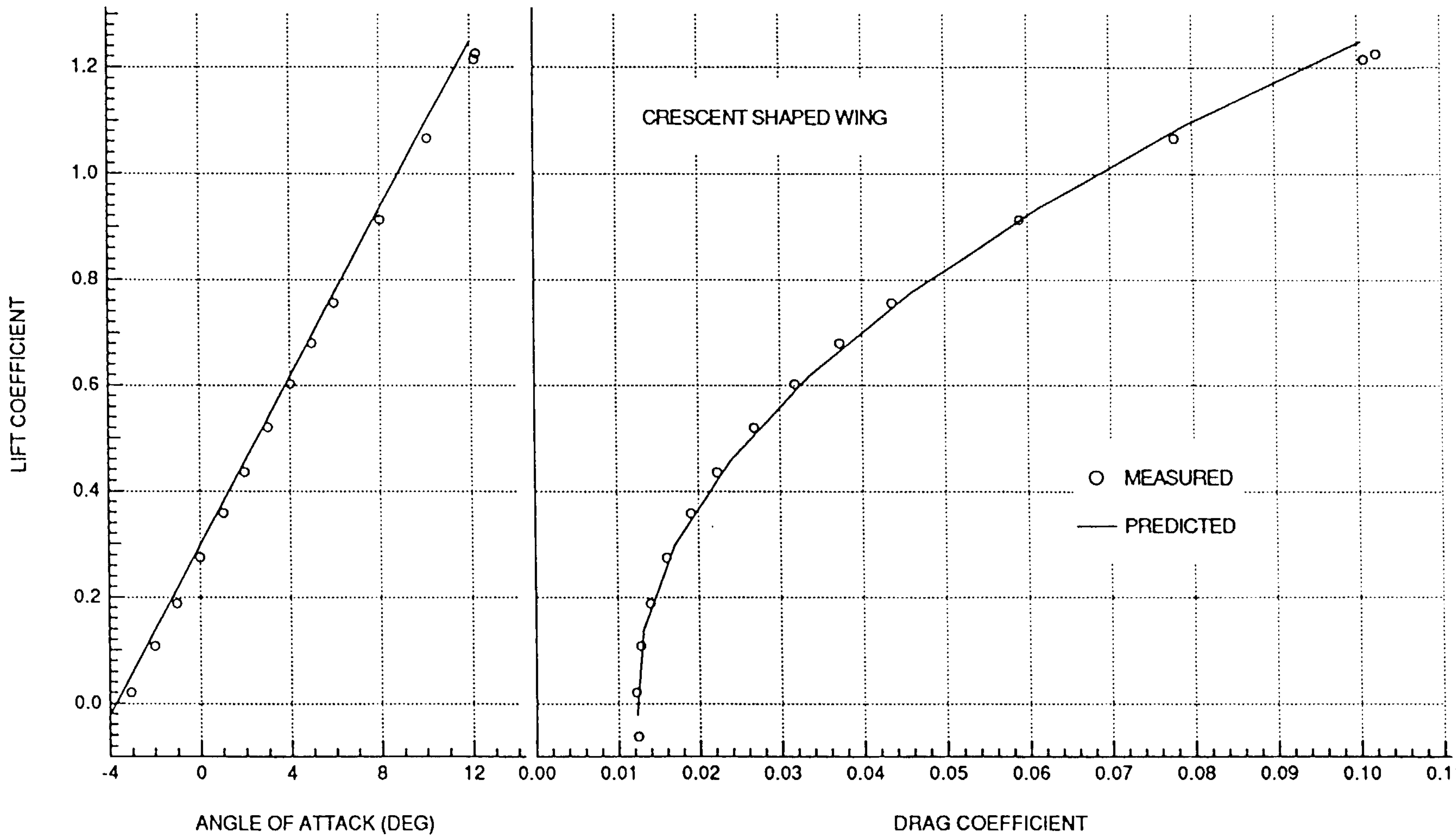

Figure 11: Comparison of the Measured and Predicted Lift and Drag of the Crescent Shaped Wing

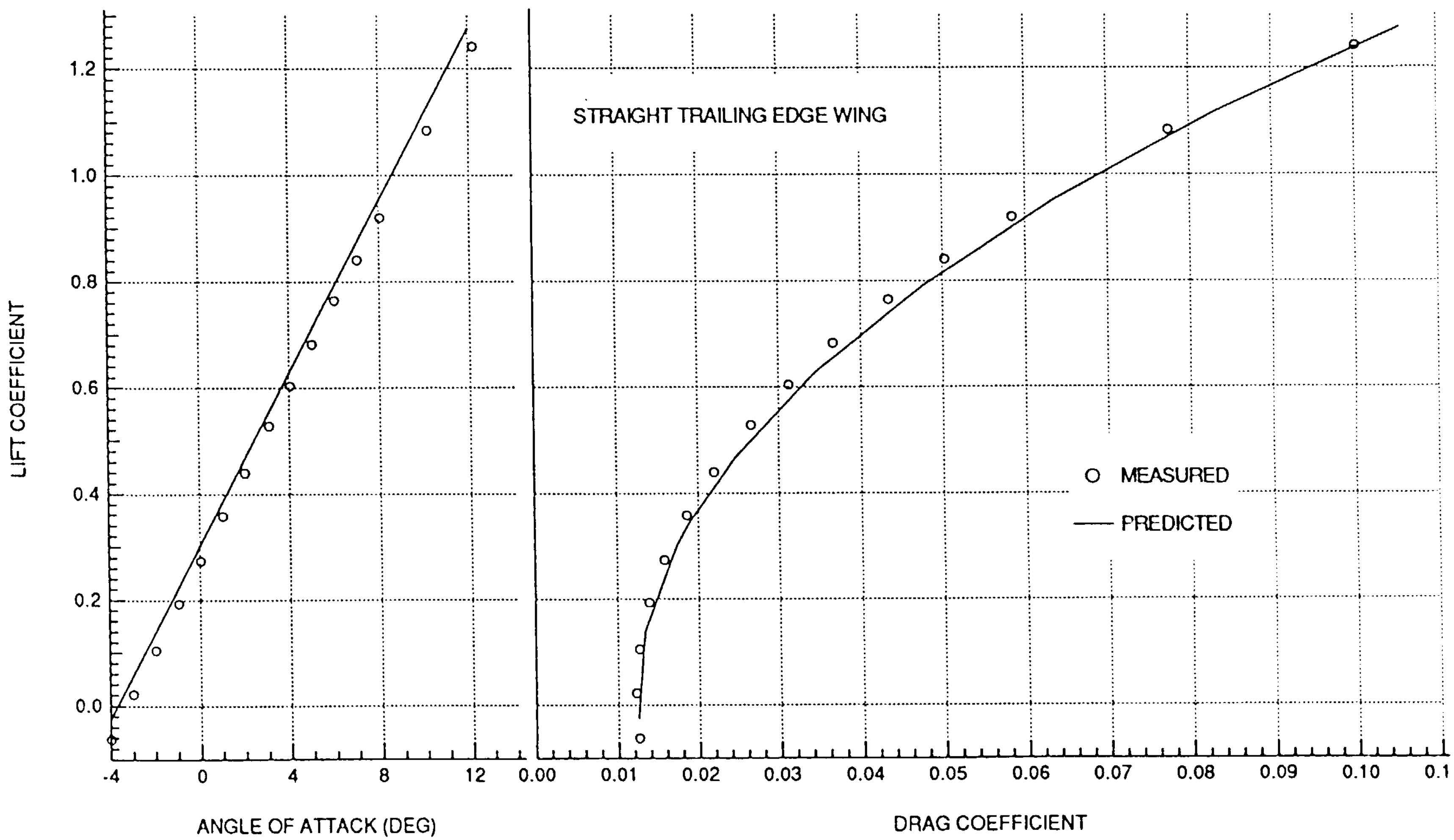

Figure 12: Comparison of the Measured and Predicted Lift and Drag of the Straight Trailing Edge Wing

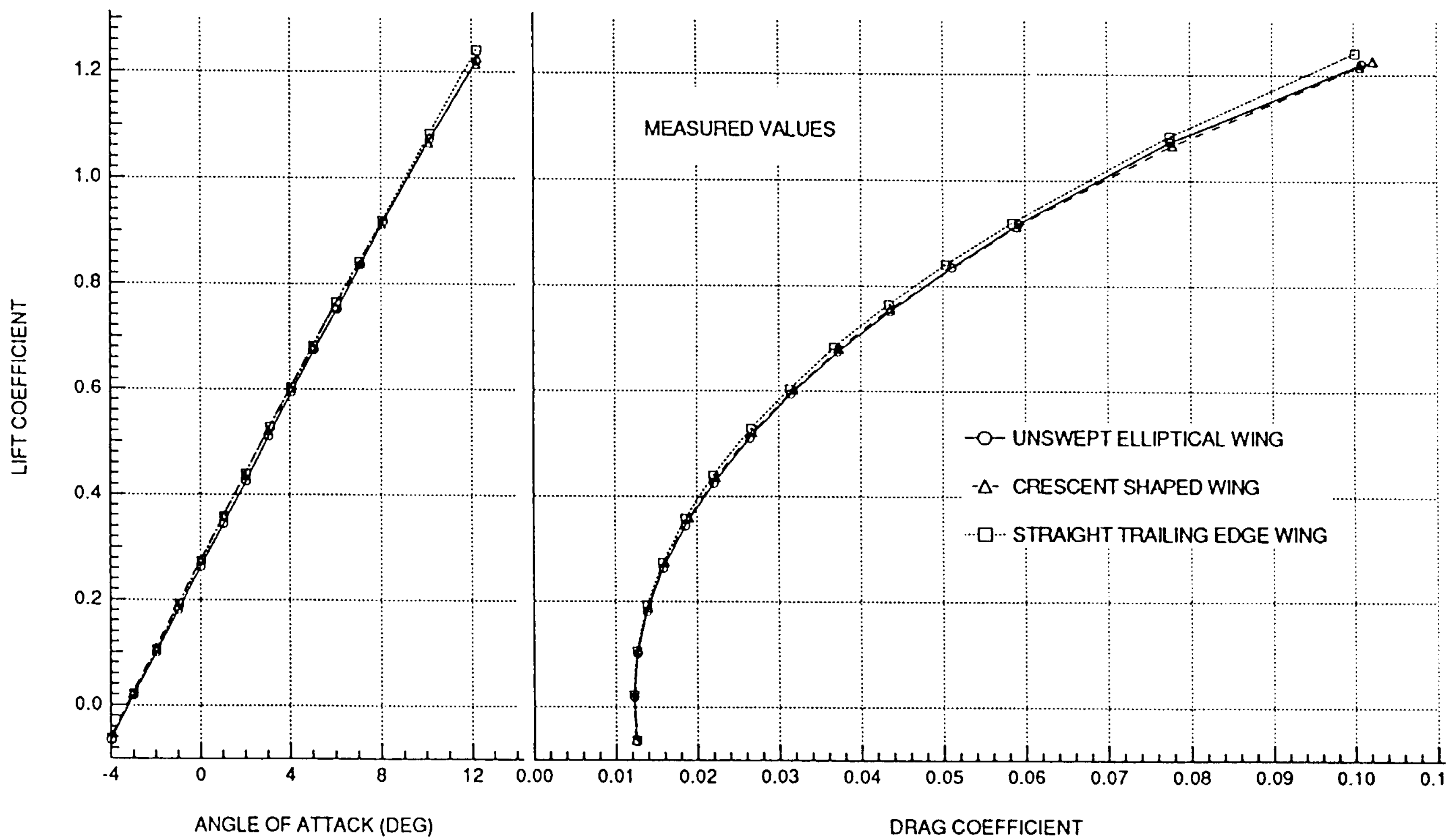

Figure 13: Comparison of the Measured Lift and Drag of the NASA LaRC Test Wings

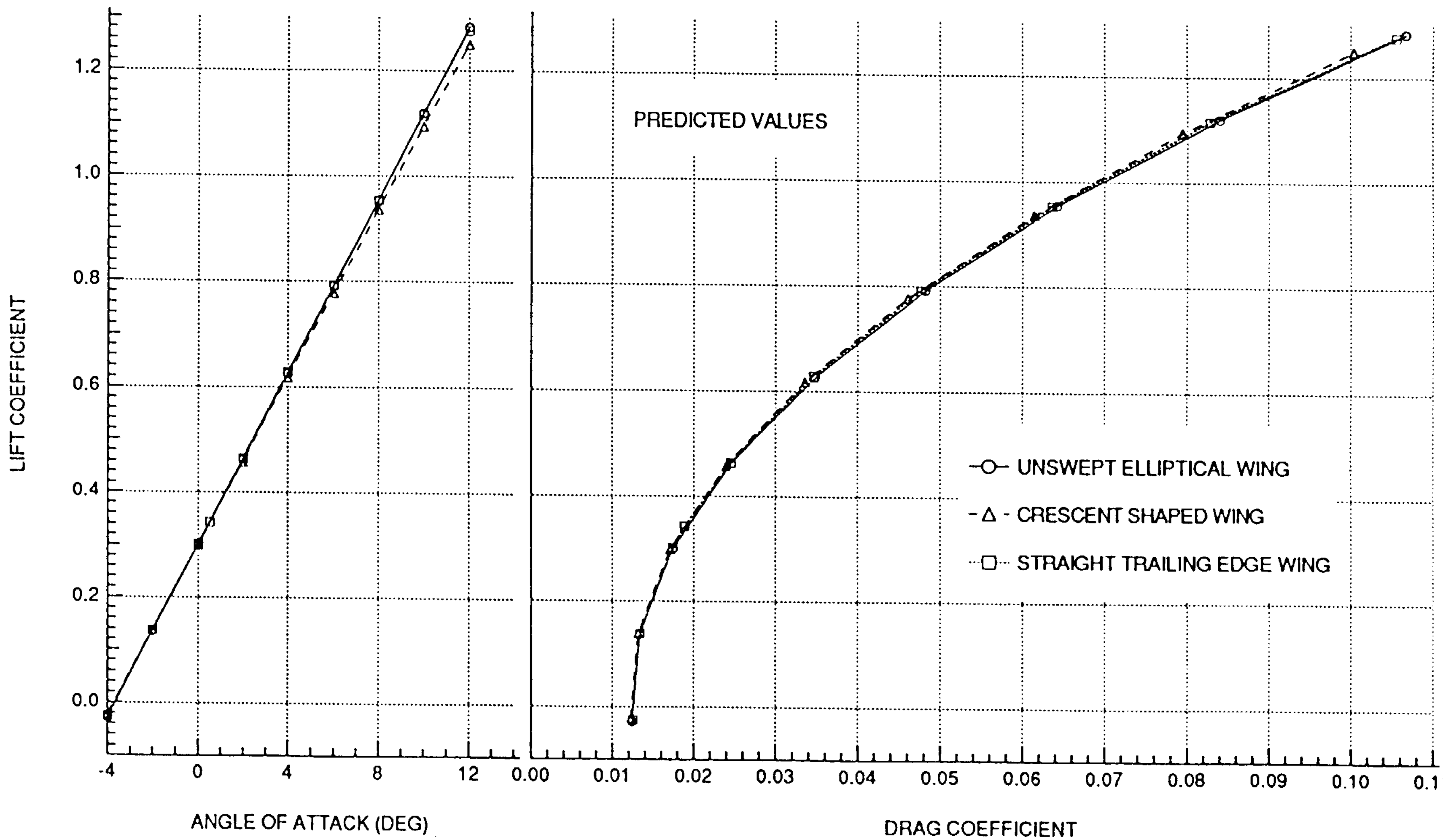

Figure 14: Comparison of the Predicted Lift and Drag of the NASA LaRC Test Wings

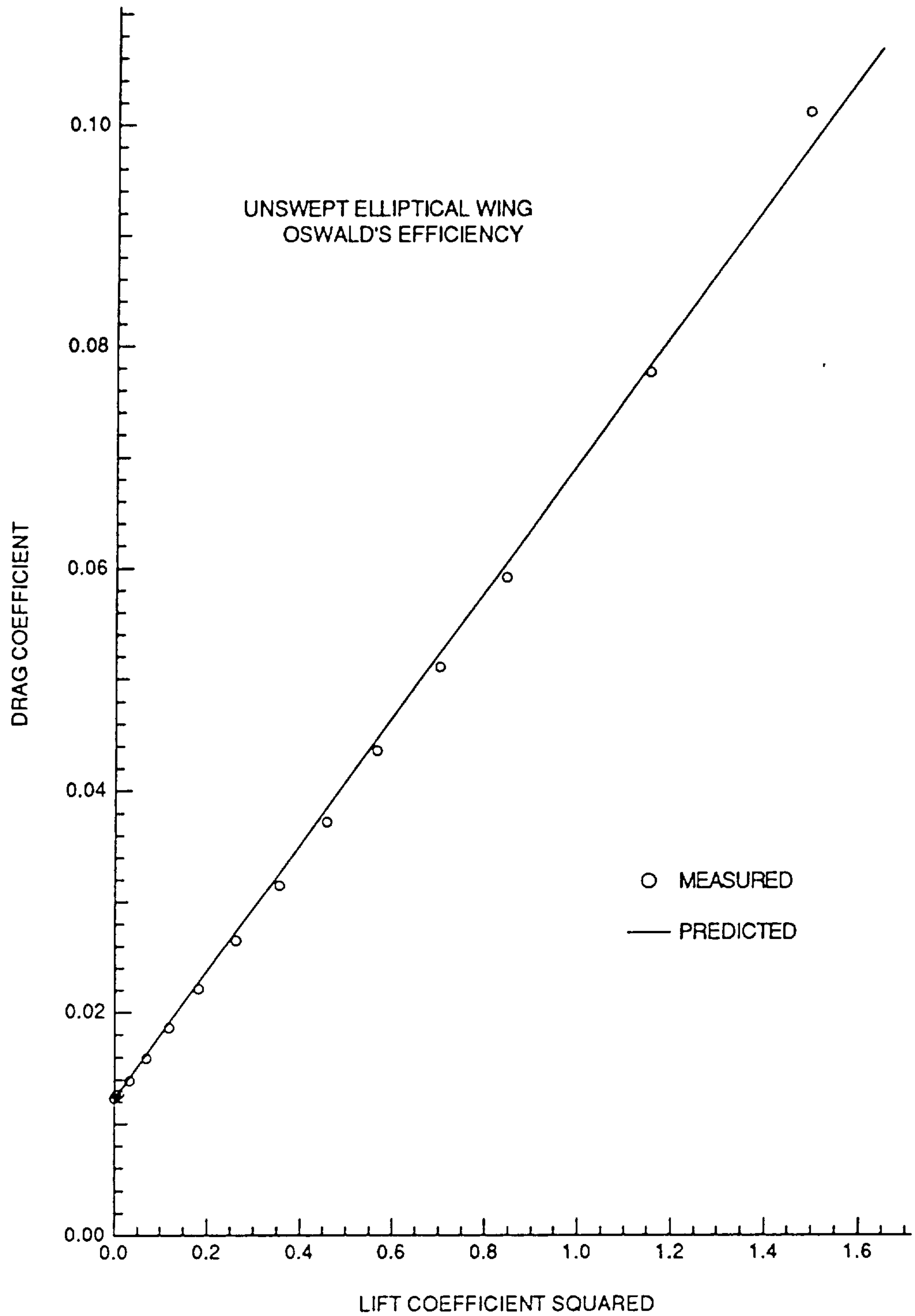

Figure 15: Comparison of the Measured and Predicted Oswald's Efficiencies for the Unswept Elliptical Wing

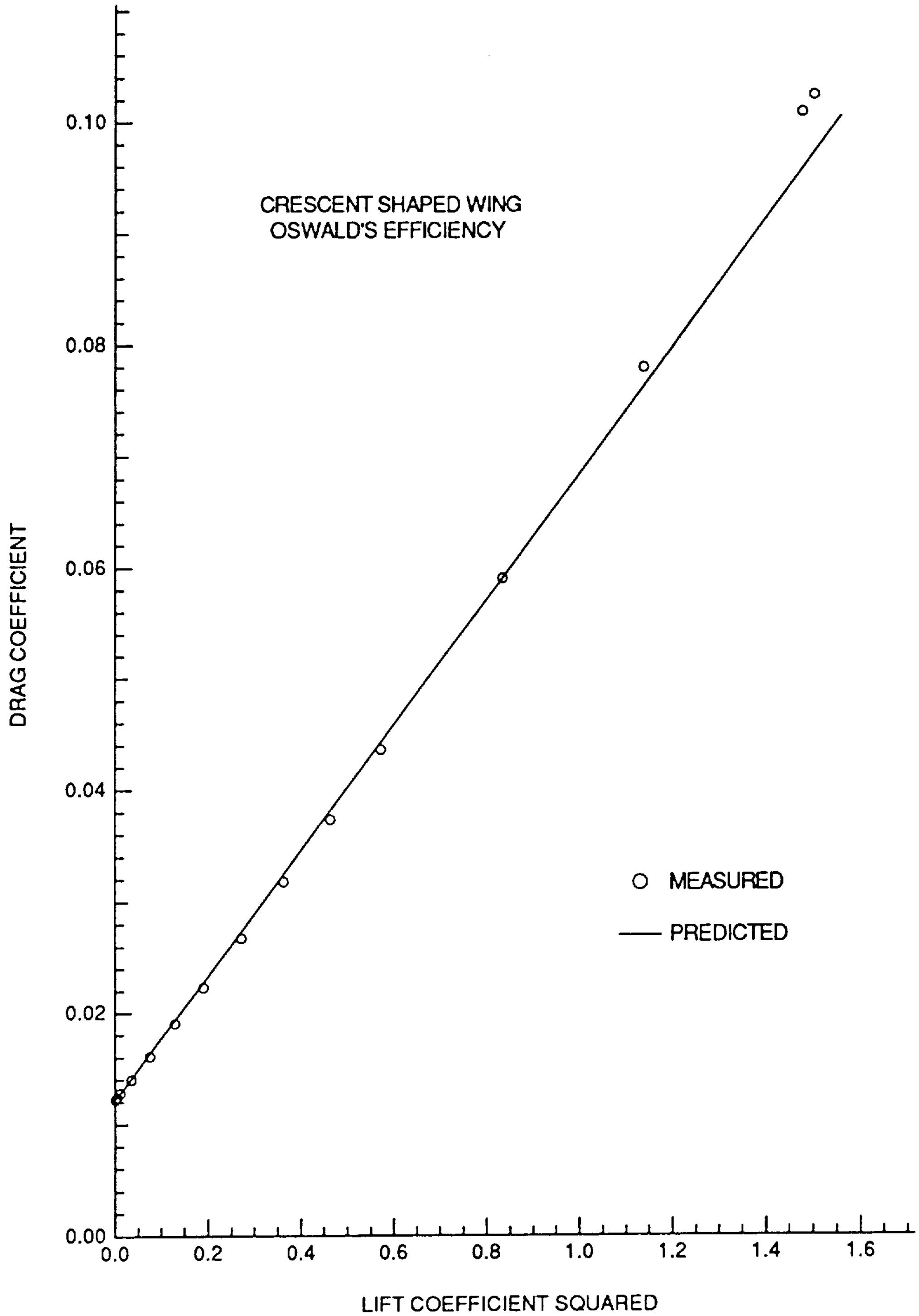

Figure 16: Comparison of the Measured and Predicted Oswald's Efficiencies for the Crescent Shaped Wing

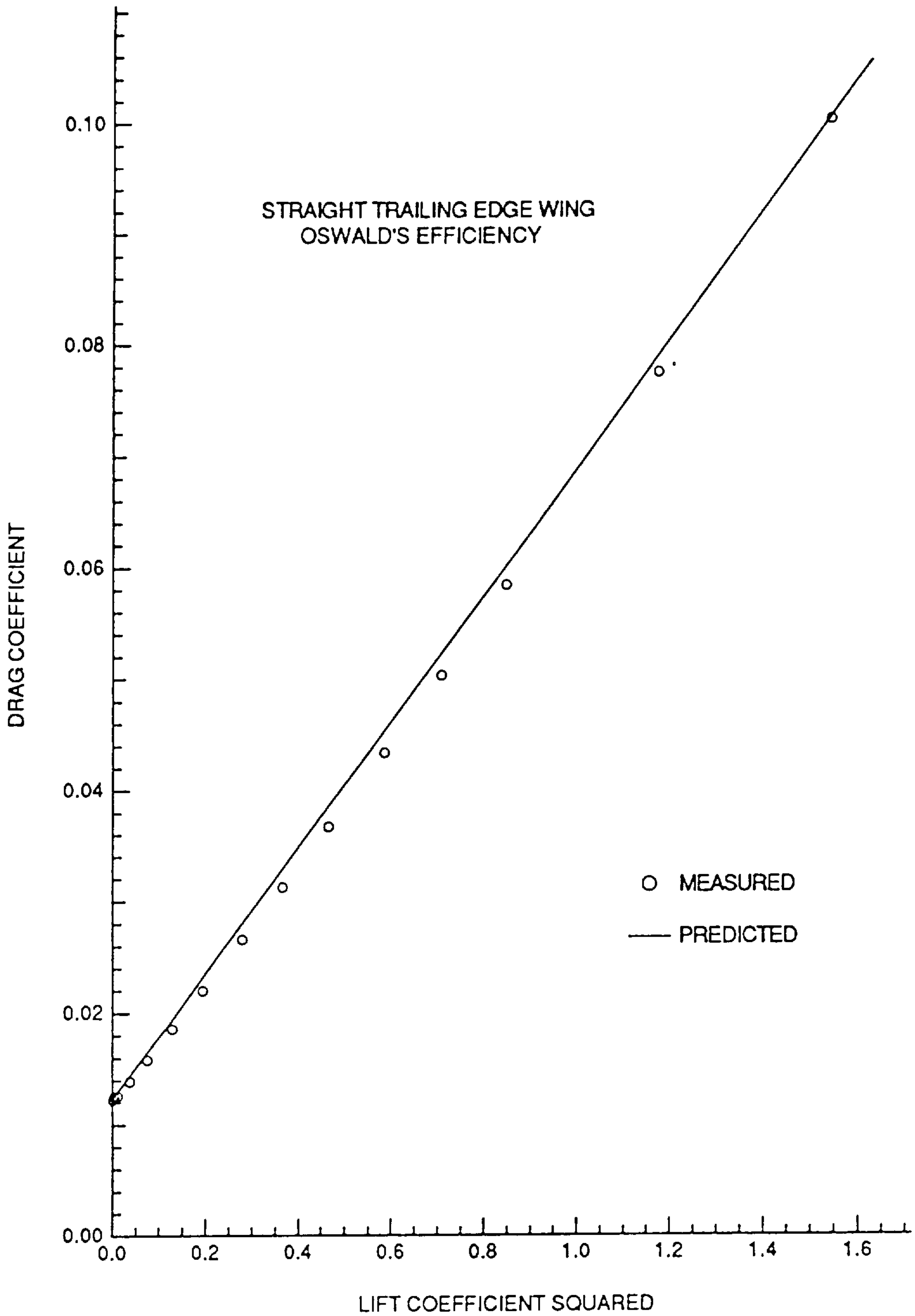

Figure 17: Comparison of the Measured and Predicted Oswald's Efficiencies for the Straight Trailing Edge Wing

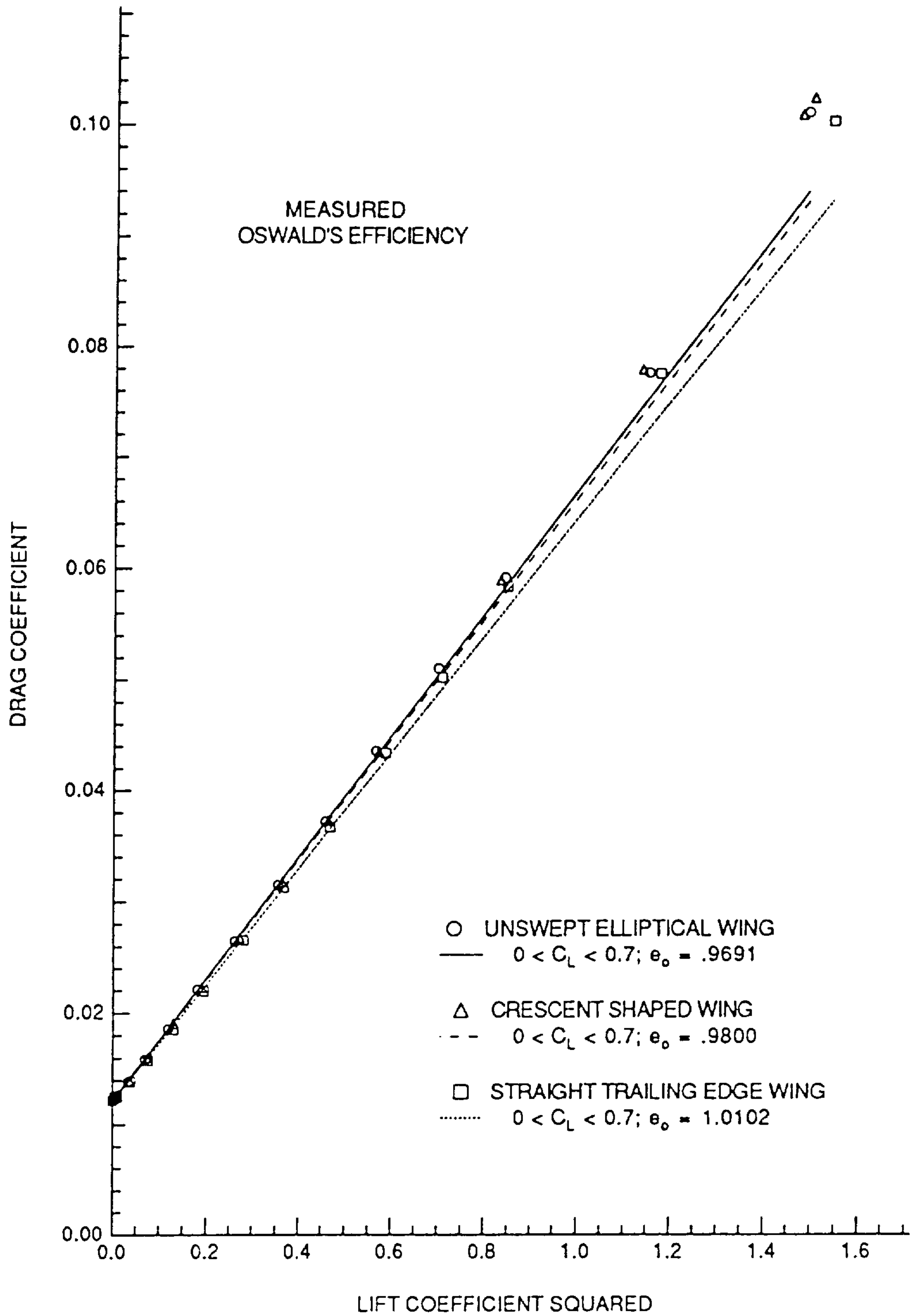

Figure 18: Comparison of the Measured Oswald's Efficiencies of the NASA LaRC Test Wings

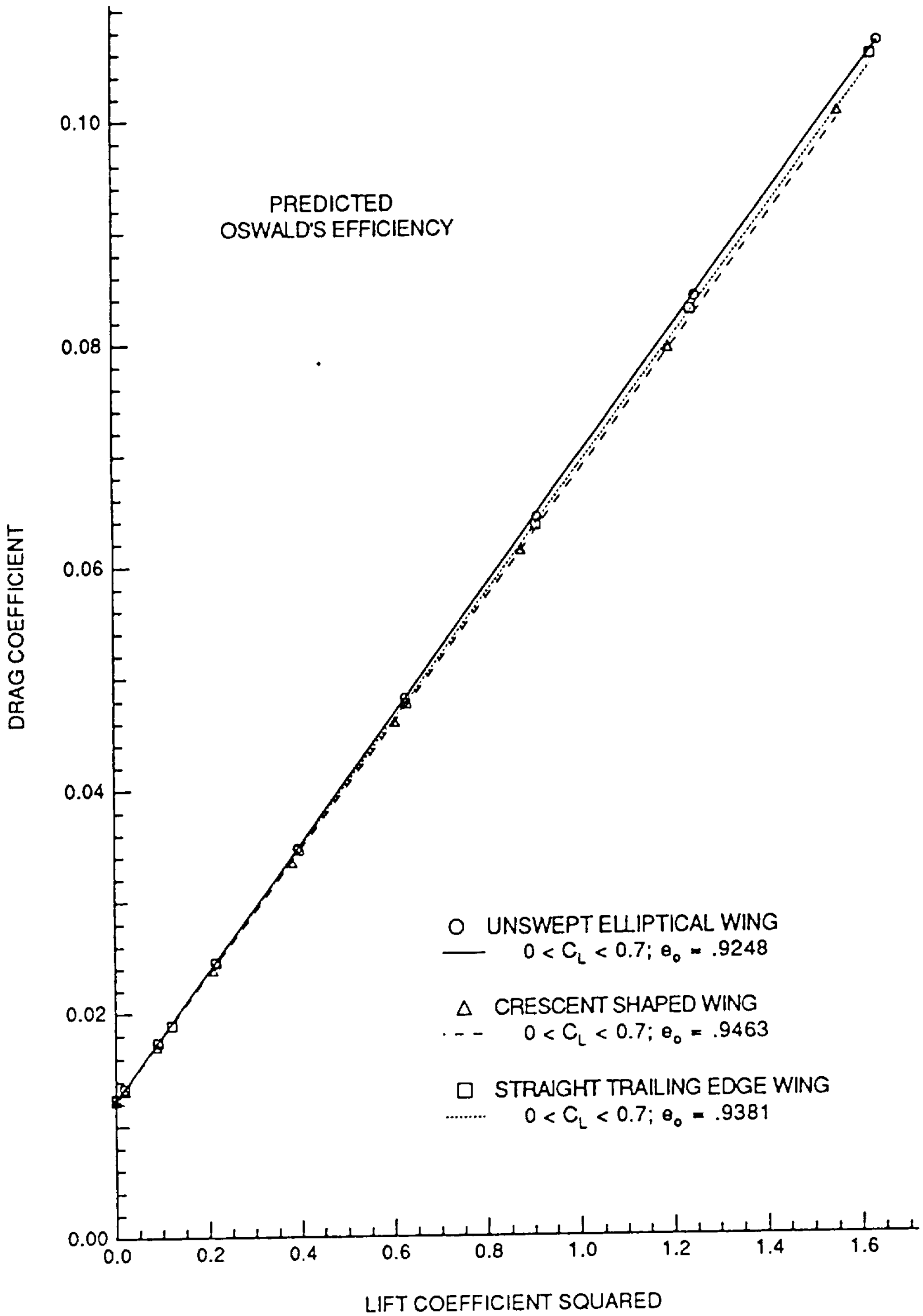

Figure 19: Comparison of the Predicted Oswald's Efficiencies of the NASA LaRC Test Wings

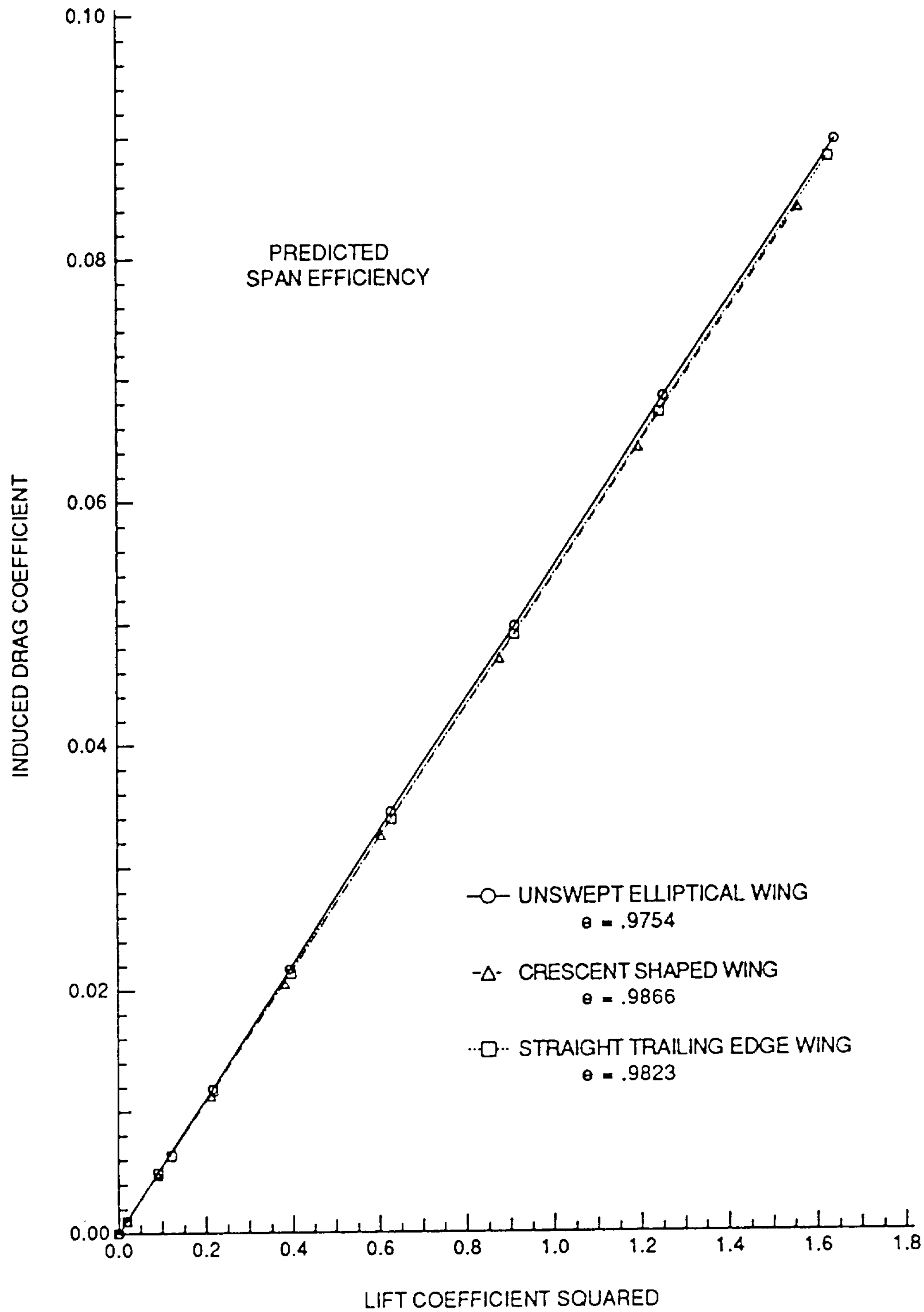

Figure 20: Comparison of the Predicted Span Efficiencies of the NASA LaRC Test Wings

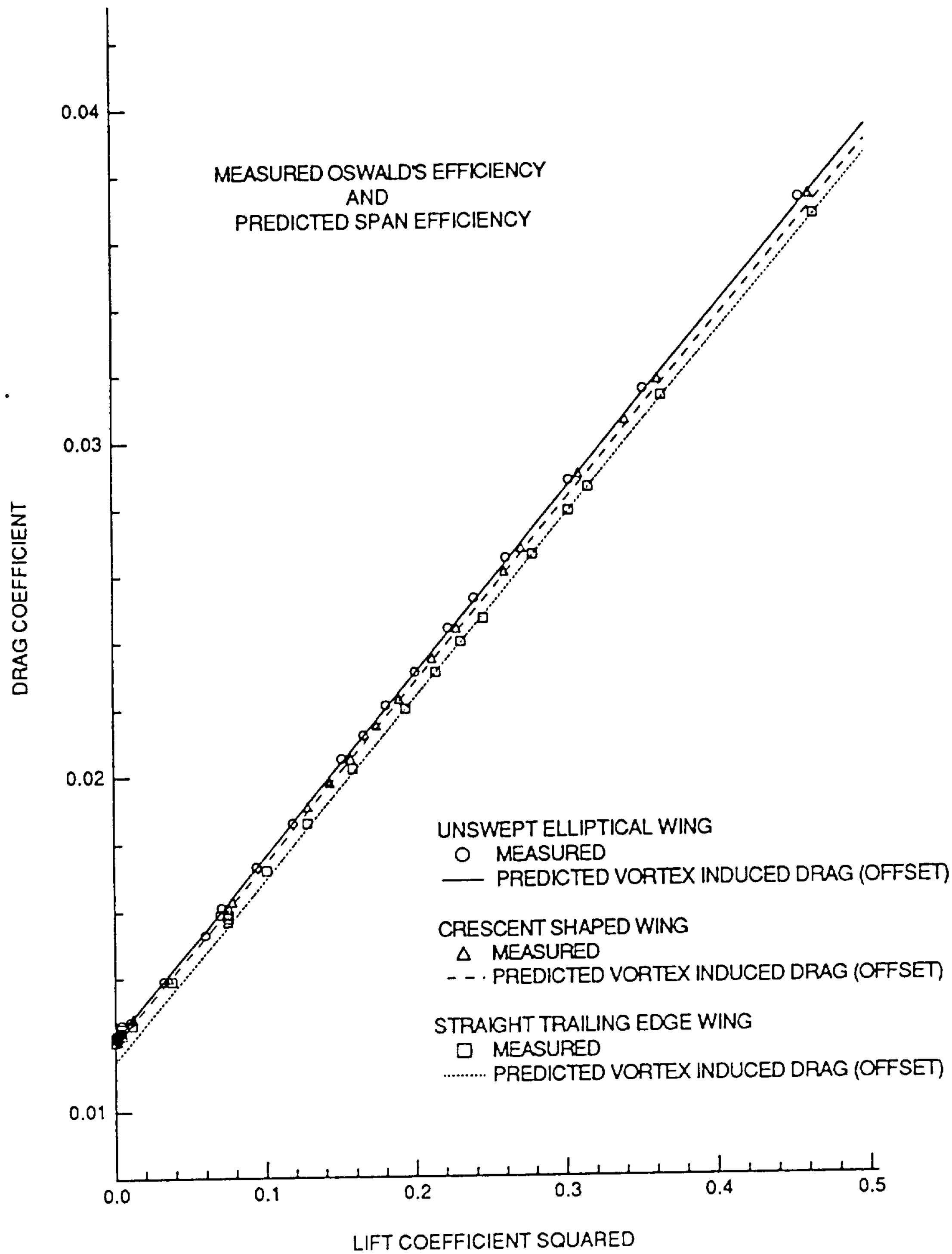

Figure 21: Comparison of Measured Oswald's Efficiency and Predicted Span Efficiency at Low Lift Coefficients for the NASA LaRC Test Wings

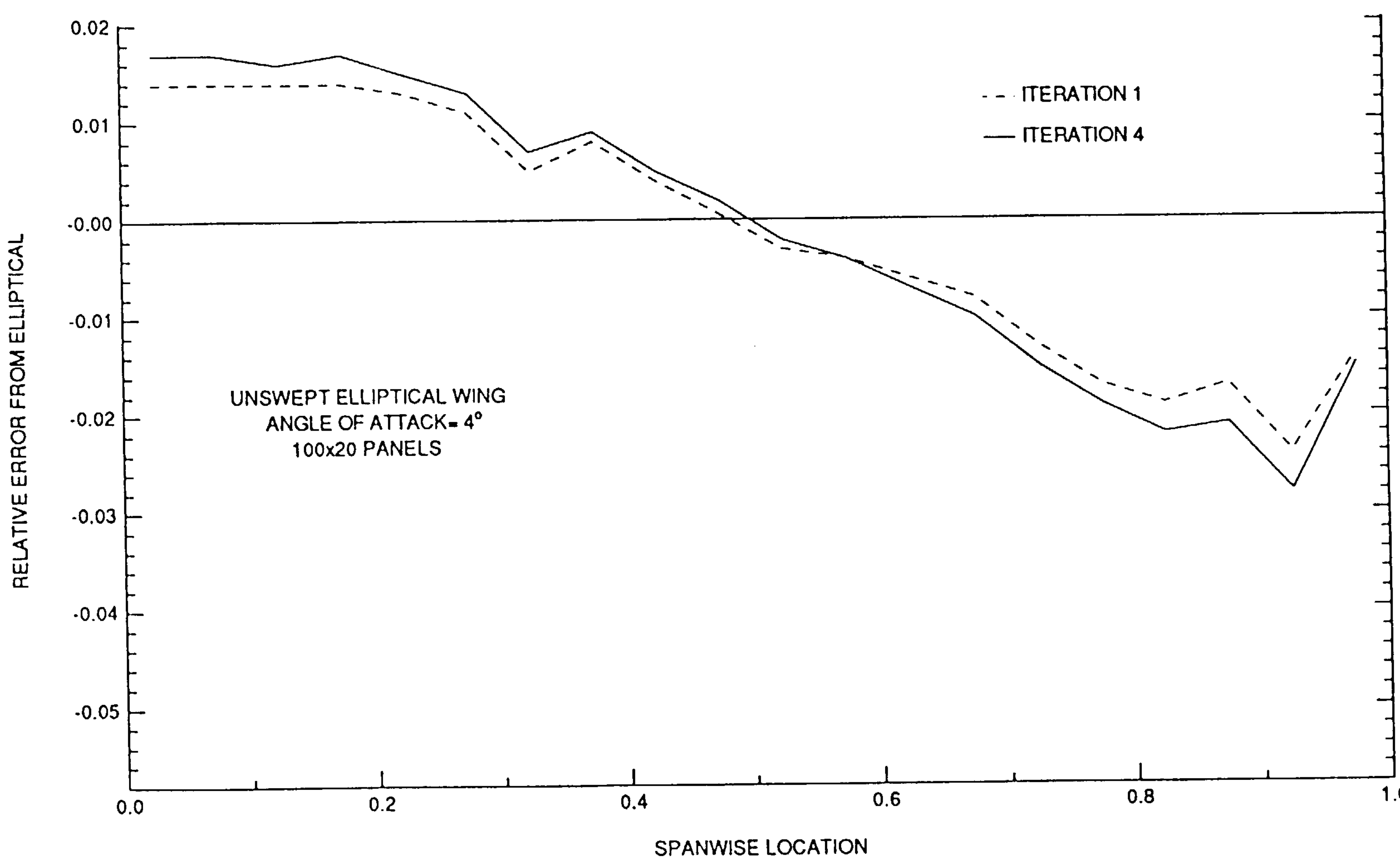

Figure 22: Effect of Wake Deformation on Spanwise Lift Distribution of Unswept Elliptical Wing

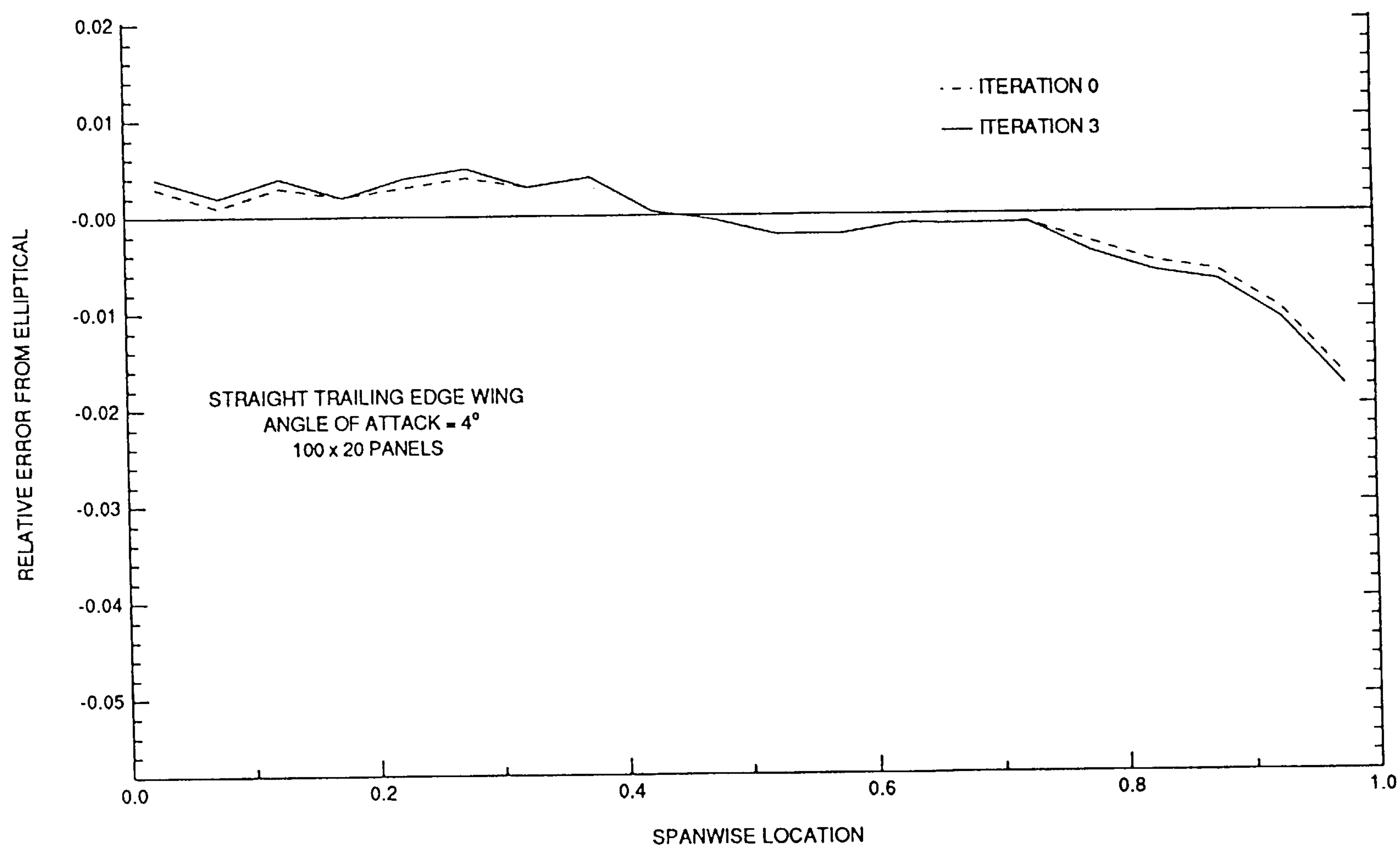

Figure 23: Effect of Wake Deformation on Spanwise Lift Distribution of Straight Trailing Edge Wing

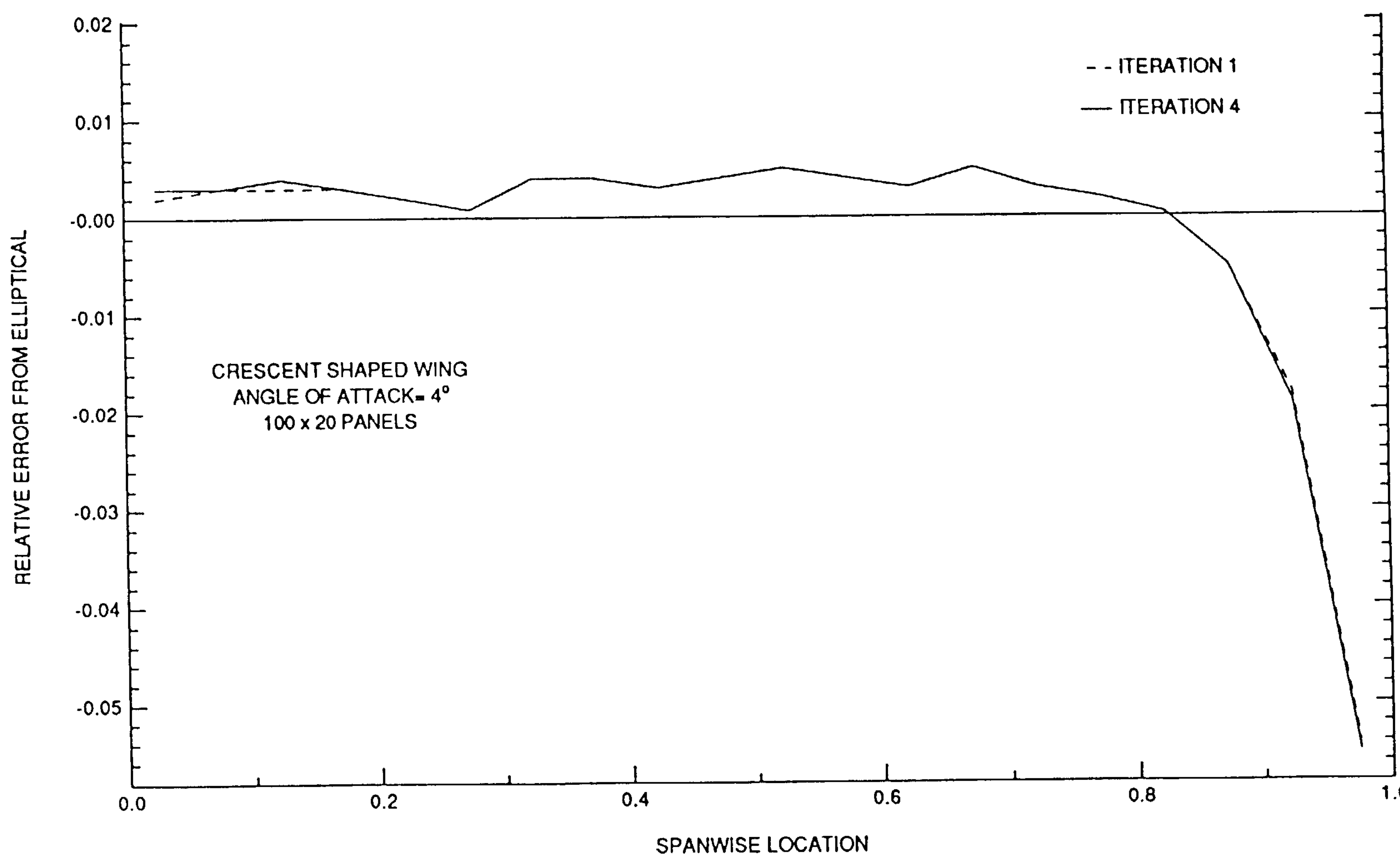

Figure 24: Effect of Wake Deformation on Spanwise Lift Distribution of Crescent Shaped Wing

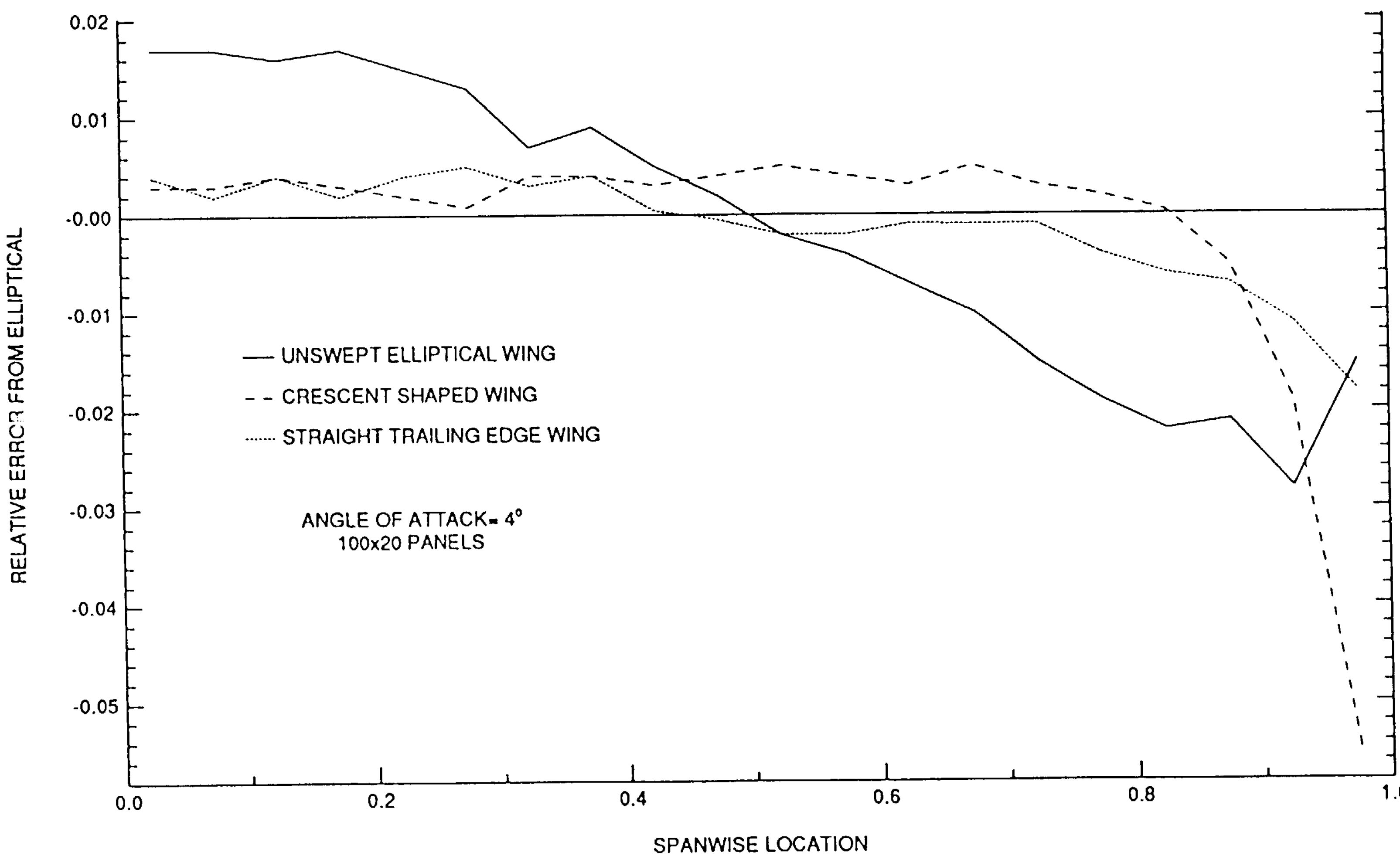

Figure 25: Effect of Wing Tip-Sweep on Spanwise Lift Distribution

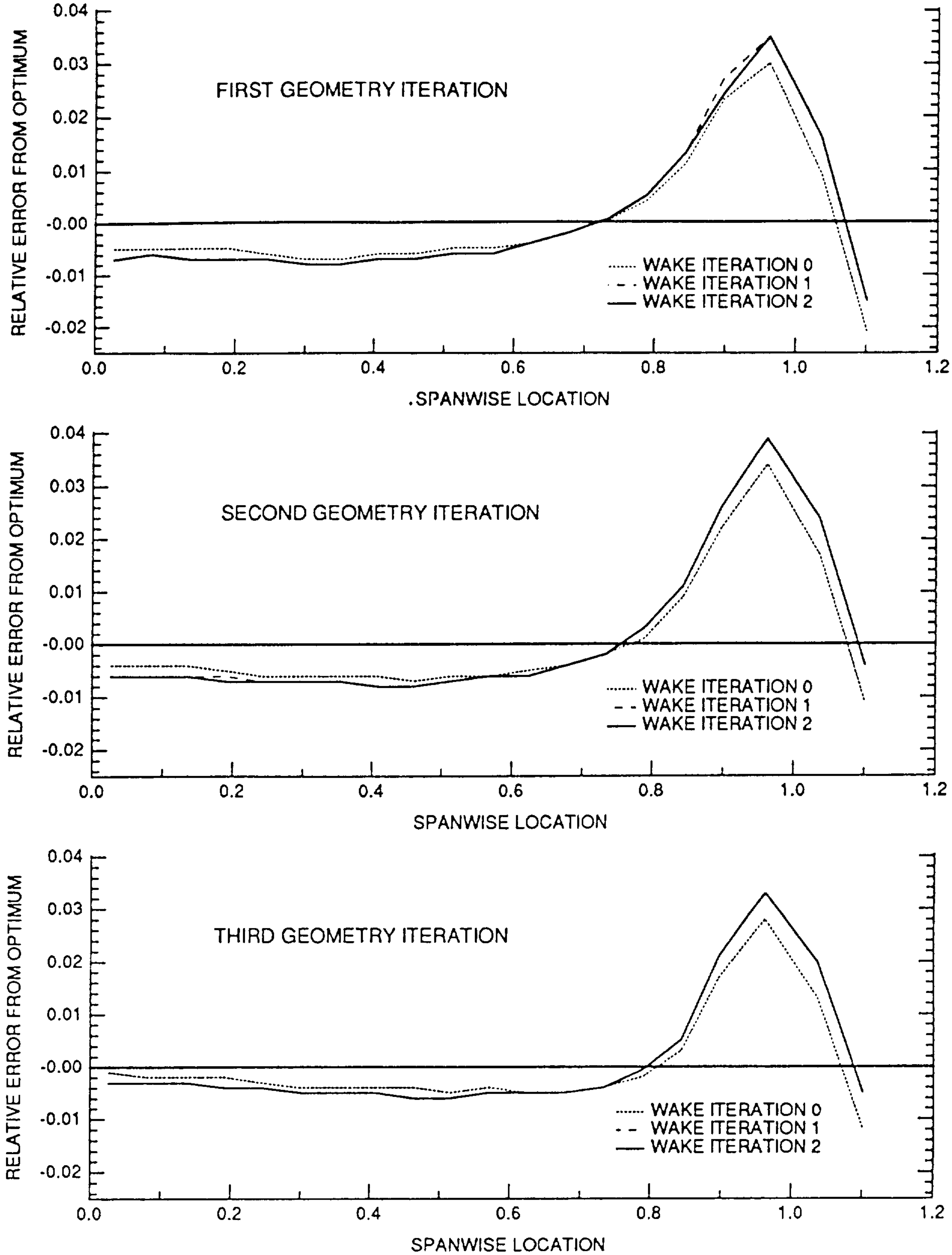

Figure 26: Non-Planar Wing Design Geometry Iterations